Available online at www.sciencedirect.com
SCIENCE DIRECT®
Computers and Structures xxx (2004) xxx–xxx
Computers & Structures
www.elsevier.com/locate/compstruc

Topology optimization for synthesis of contact-aided compliant mechanisms using regularized contact modeling

Nilesh D. Mankame, G.K. Ananthasuresh *

Mechanical Engineering and Applied Mechanics, University of Pennsylvania, 297 Towne Building, 220 South 33rd Street, Philadelphia, PA 19104-6315, USA

Received 25 June 2003; accepted 10 February 2004

Abstract

A topology optimization technique for systematically designing contact-aided compliant mechanisms (CCM) is presented in this paper. A CCM is a single piece elastic body that uses intermittent contacts in addition to elastic deformation to transmit force and motion. Contact interactions give rise to interesting nonlinear and nonsmooth behaviors even under the small deflection assumption made in this work. The difficulties associated with the nondifferentiability inherent in the CCM systematic synthesis problem are circumvented by using a regularized contact model. This model uses a smooth approximation of the unilateral displacement constraints that are used to model contact interactions. The use of a regularized contact model in the underlying state problem makes it possible to use efficient smooth optimization algorithms for the systematic synthesis of CCMs. The formulation of the design problem for CCMs, sensitivity analysis, and solution methodology are presented. The paper includes CCM designs that exhibit nonsmooth motion and force transmission characteristics, which are not possible or practical with compliant mechanisms that do not use intermittent contact interactions.

Keywords: Topology optimization; Regularized contact; Compliant mechanisms; Nonsmooth function generation; Systematic synthesis

1. Introduction

Compliant mechanisms (CMs) are single-body, elastic continua that are designed to deform as desired upon application of forces. Like jointed, rigid-body mechanisms, CMs transmit and transform force and motion. The use of CMs in place of rigid-body mechanisms brings many advantages in performance and manufacturing [1–3] to some applications, especially at the microscale. The benefits related to the performance include reducing or eliminating friction and backlash due to the absence of kinematic joints. The manufacturing advantages include assembly-free single-body construction, scalability for microsystems applications, and amenability for nonmechanical actuation [2,4]. CMs have already been used in many applications in MEMS, adaptive structures, surgical tools, etc. Their superiority over rigid-body mechanisms for applications requiring high repeatability or compact and scalable designs notwithstanding, CMs are yet to be endowed with additional characteristics that rigid-body mechanisms possess. Such features include: a wider variety of motion and force transmission characteristics, acceptable performance at high speeds and resistance to yielding, fracture and fatigue. Contact-aided compliant mechanisms (CCMs) address the first aspect as explained below.

Currently available single-body compliant mechanisms can only generate smooth output paths and

* Corresponding author. Tel.: +1-2158987191; fax: +1-2155736334.
E-mail addresses: nileshdm@seas.upenn.edu (N.D. Mankame), gksuresh@seas.upenn.edu (G.K. Ananthasuresh).

0045-7949/$ - see front matter © 2004 Elsevier Ltd. All rights reserved.
doi:10.1016/j.compstruc.2004.02.024

force–deflection characteristics with monotonic continuous input forces if buckling and sudden changes in the constitutive properties of the material are not permitted. This is a direct consequence of the smoothness of the displacement field in an elastic continuum. In contrast, the vast variety of nonsmooth motions possible with rigid-body jointed mechanisms is well known [5]. In order to endow compliant mechanisms with similar kinematic and kinetostatic capabilities, *contact-aided compliant mechanisms* (CCMs) were introduced by Mankame and Ananthasuresh [6]. The enhanced capabilities were made possible by intermittent contact between different parts of the elastic body or between an elastic body and a rigid surface.

The focus of this paper is on the systematic synthesis of CCMs for prescribed nonsmooth response using the topology optimization technique. Section 2 highlights the ability of CCMs to extend the functionality of compliant mechanisms via examples of existing designs that embody the CCM concept. Although topology optimization for the synthesis of CMs has been widely researched in the past decade ([7] and the references therein), the extension of this technique to the problem of systematically synthesizing CCMs is not straightforward.

The analysis of an elastic body undergoing intermittent contact interactions involves unilateral constraints on displacements. These constraints are a form of nonlinear mixed boundary conditions, wherein both the extent of the actual contact boundary and the contact reaction on this boundary are unknown a priori. In addition to a strong nonlinearity, these constraints also introduce nondifferentiability into the response of an elastic body that experiences contact interactions during the course of its deformation. The nondifferentiability of the output response can be readily appreciated by noting that due to a change in the boundary conditions, two different boundary value problems (BVP) govern the behavior of the elastic body before and after it contacts another body. Moreover, there exists a transition state at which the switchover between the two BVPs takes place. At the transition state, it is not possible to determine the change in the response of the system to a small perturbation of the system parameters, without knowing the *direction* of the perturbation. In other words, the state of the system is *only directionally differentiable* at the transition state [8–11]. This aspect is discussed in Section 3.

There exists a rich body of literature on the optimal design involving contact interactions in applications pertaining to design of railwheels and track profiles, bearings and structural supports. There has also been considerable recent work on structural optimization including unilateral constraints. Section 3 contains a brief overview of the literature relevant to this work and places the contribution of this work in the context of the past research in related areas.

The nondiffenrentiable or nonsmooth behavior of the system warrants nonsmooth analysis techniques to establish the existence of a solution and study its properties. The nonsmoothness, unless remedied in some way, precludes the use of well-developed gradient-based smooth optimization techniques in the systematic synthesis of CCMs. A contact-smoothening technique, called *regularization* for the reasons to be explained later, is introduced to circumvent the above problem in this work. The idea underlying this technique is explained in Section 4.

Section 5 describes the formulation of the topology synthesis problem for the design of a CCM. Section 6 contains a brief description of the sensitivity analysis and the solution procedure used to solve this problem.

The work reported in this paper is limited to frictionless and adhesionless contact of an elastic body with rigid external contact surfaces. Small deflections and a linear elastic material behavior are also assumed. The first two assumptions reduce the complexity of the contact analysis problem without significantly reducing its usefulness. The last two assumptions make it possible to isolate the effects of contact interactions from other sources of nonlinearity and nonsmoothness. Under these assumptions, the nonsmooth behavior is only due to the intermittent contacts and not due to frictional stick/slip, geometric nonlinearity of the structure or to a sudden change in the material behavior. The examples of novel CCMs reported in Section 7, demonstrate that interesting behavior and practically useful mechanisms are not precluded by these assumptions. Discussion of the results and future extensions of this work are covered in Section 8 followed by concluding remarks in Section 9.

2. Contact-aided compliant mechanisms

Consider a cantilever beam with load acting at a point between the fixed end and the free end. Let there be a semicircular rigid external surface underneath as shown in Fig. 1. As the force F is increased, the beam deflects and eventually, contacts the rigid surface. This introduces a contact reaction, which changes the mode of deformation of the beam. Three configurations of the beam, viz., undeformed (A), deformed before the contact (B), and deformed after the contact (C), are shown in the figure. It is easy to see that, the vertical deflection of the tip (δ), as a function of the applied force (F) is nonsmooth: the tip initially moves down, abruptly changes its direction upon contact, and rises up thereafter with increasing values of F. This simple example illustrates how an intermittent contact can give rise to interesting nonsmooth motions using single-piece elastic bodies. It is important to note that the rigid surface does

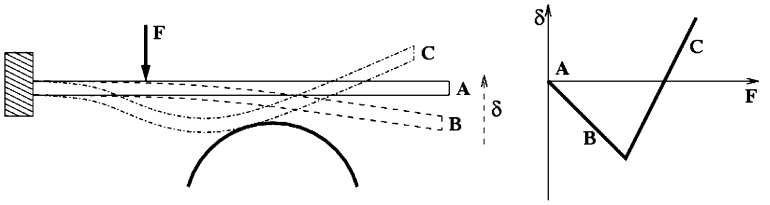

Fig. 1. Nonsmooth force–deflection behavior from a cantilever beam contacting a rigid surface.

not count as an additional body; it is an extension of the portion to which the elastic body is anchored. Two examples of existing product designs that embody the concept of CCMs are presented below to further illustrate the operating principle underlying CCMs.

A hand-held dental floss tool is shown in Fig. 2. It is a commercial product that is about 5 cm long and is made of a plastic material. The floss F is initially slack. When a force is applied as shown, points A and B move apart by pivoting about the flexure connection (P) to pull the floss taut. This also causes points C and D to move closer. Further application of the force brings C and D into contact. This contact stiffens the mechanism and prevents further tensioning of the floss to prevent its breakage. In the floss tool, the contact with a rigid surface in the cantilever example is replaced by the self-contact, which restricts the post-contact motion. This simple device shows how an intermittent contact can alter the stiffness of the mechanism to serve a functional purpose.

An elastic body with fixed boundary conditions (i.e., ordinary compliant mechanisms) under a continuous monotonic input force will not be able to provide the behavior depicted in the above example. The stiffening of the mechanism seen in the dental floss tool may be achievable by geometric stiffening but then the device would experience high stresses. Saxena and Ananthasuresh [12] and Pedersen et al. [13] encountered nonsmooth behaviors in large-deformation compliant mechanism design. This unintended nonsmooth behavior was attributed to a buckling type local collapse of a part of the mechanism body. Such nonsmoothness arising from structural instability is not only difficult to control but also impractical. In contrast, CCMs can be designed to achieve arbitrary nonsmooth behaviors within the small deflection limits imposed by linear elasticity, without loss of structural stability and without exceeding the material strength.

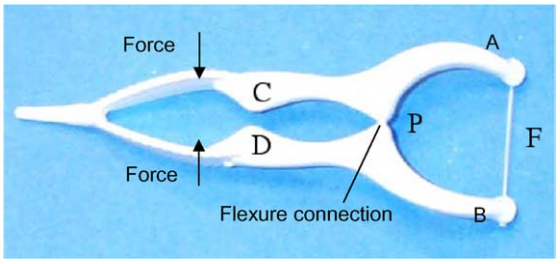

Fig. 2. Dental floss tool as an example of a CCM that undergoes an abrupt change in stiffness.

Consider another example of an intuitively designed CCM, which involves contact at three points with a rigid surface as well as a self-contact. As shown in Fig. 3, this device generates two sharply curved arches that enclose an area using a single, continuous, reciprocating, translatory input. In Fig. 3a, the geometry and locations of the input port, the output ports, and the contact regions are shown. When the input point I is pulled to the left, the elastic body of the mechanism deforms and points C2 and C3 touch the straight segments adjacent to them. These two self-contacts create a sharp change in the output paths traced by P and P′. Pulling point I farther to the left bring point C1 in contact with the rigid surface shown as an oval in the figure. This increases the stiffness of the mechanism and thereby enables it to bear the output loads, if any. The self-contact also redistributes the strain energy evenly throughout the deforming segments to avoid material failure. When point I is released, the two output curves are re-traced bringing the mechanism to the original configuration. The curves for P and P′ predicted by nonlinear finite element simulation are shown in Fig. 3b. A polypropylene prototype actuated by a linear stepper motor connected to point I is shown in Fig. 3c. By attaching pencil leads at each output point, the output paths were traced as shown in Fig. 3d. The experimentally obtained curves bear close resemblance with the simulated ones in Fig. 3b. The discrepancy between the experimental and simulation results is attributed to viscoelastic material behavior and frictional output loads, which were not accounted for in the simulations. This device is intended for use in automated isolation and capture of single cells from biological tissue [14].

The CCMs described above were designed intuitively. The objective of this paper is to develop systematic methods to design such devices for a specified nonsmooth behavior in terms of either the force–deflection characteristics or the output path.

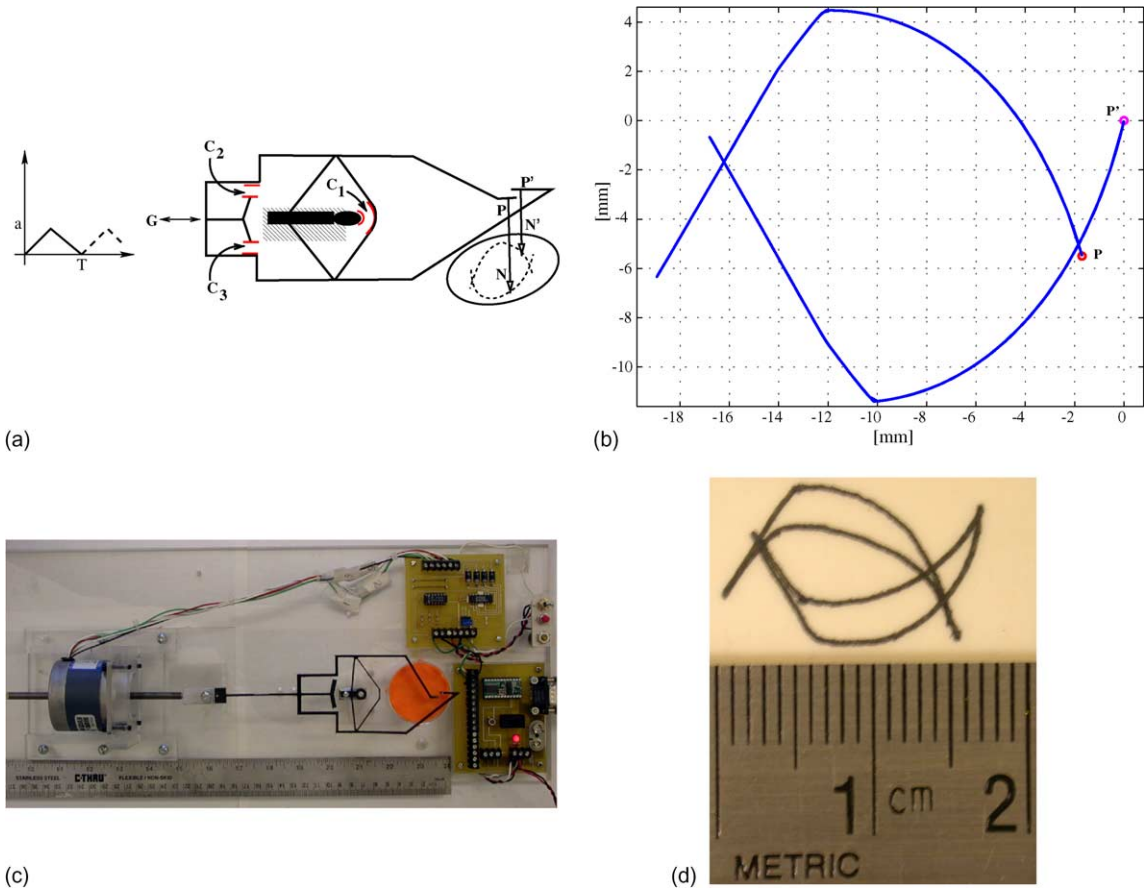

Fig. 3. A CCM with three contacts to generate a pair of sharply curved arches: (a) schematic, (b) the simulated curves without the output load at the points, (c) polypropylene prototype driven by a stepper motor, (d) curves obtained from the experiment.

3. Theoretical background and related work

This work is concerned primarily with *Signorini contact* [15], i.e., frictionless and adhesionless contact of an elastic body with a semi-infinite rigid obstacle. The Signorini BVP governs the behavior of a CCM such as the first example in Section 2. The approaches that have been used to solve this problem are briefly reviewed in Section 3.1. The emphasis is on their suitability for use in an optimization framework. This is followed by an overview of optimal design problems involving contact with a focus on structural optimization.

3.1. Signorini contact

Let B be an elastic body that can potentially contact a semi-infinite rigid wall W as shown in Fig. 4. The boundary of B consists of three disjoint parts: S_d where the displacement u^0 is specified, S_f on which an external force f is applied, and S_C at which contact with W may take place. Let $g(\mathbf{x})$ denote the initial gap between a point $\mathbf{x}$ on S_C and a corresponding point on the wall W. A unit vector normal to W is denoted by $\hat{\mathbf{n}}$. Under the assumption of small deflections, the displacement $\mathbf{u}(\mathbf{x})$ and the stress $\boldsymbol{\sigma}(\mathbf{x})$ at every point in B must satisfy the following equations for static equilibrium:

$$\begin{aligned} &\sigma_{ij,j}(\mathbf{x}) + b_i(\mathbf{x}) = 0 \quad \forall \mathbf{x} \in B, \\ &\varepsilon_{ij}(\mathbf{x}) = \frac{1}{2}(u_{i,j}(\mathbf{x}) + u_{j,i}(\mathbf{x})), \\ &\sigma_{ij} = E_{ijkl}\varepsilon_{kl}, \end{aligned} \tag{1}$$

$$u_i(\mathbf{x}) = u_i^0 \quad \forall \mathbf{x} \in S_d, \tag{2}$$

$$\sigma_{ij}(\mathbf{x})n_j(\mathbf{x}) = f_i(\mathbf{x}) \quad \forall \mathbf{x} \in S_f, \tag{3}$$

$$\left.\begin{array}{c} -u_n(\mathbf{x}) - g(\mathbf{x}) \leqslant 0 \\ \sigma_n(\mathbf{x})(u_n(\mathbf{x}) + g(\mathbf{x})) = 0 \\ \sigma_n(\mathbf{x}) \geqslant 0 \end{array}\right\} \forall \mathbf{x} \in S_C, \tag{4}$$

where $\boldsymbol{\varepsilon}$ is the strain, $\boldsymbol{E}$ is the tensor embodying the constitutive elastic properties of the material, and the

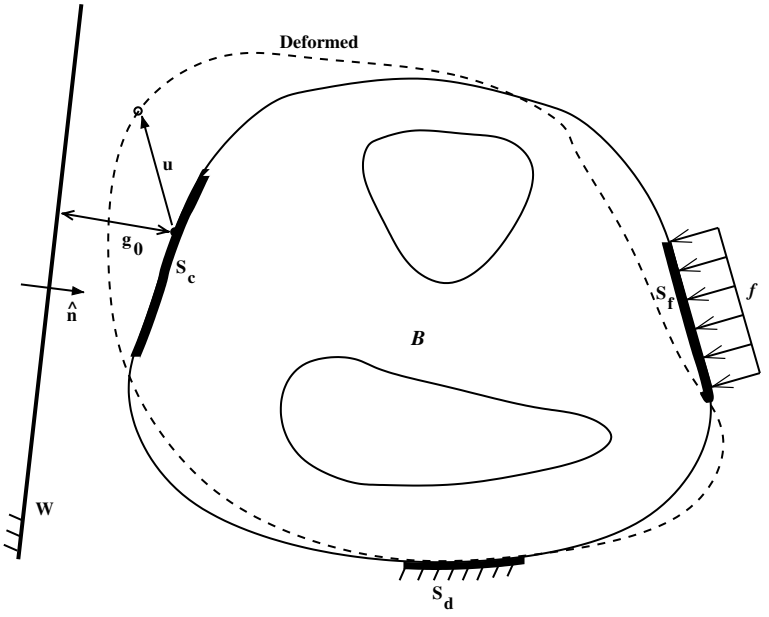

Fig. 4. Schematic description of the Signorini's contact problem.

subscript n denotes the component in the direction of $\hat{\mathbf{n}}$. The three component equations of Eq. (4), model the contact condition by ensuring the *unilateral* (i.e., one-sided) nature of the contact, the *complementarity* between the gap after the deformation and the contact stress (i.e., either the gap is open and the contact stress is zero or the gap is closed and the contact stress is non-zero), and the *nonnegativity* of the contact stress, respectively.

The above set of equations can also be obtained as the first order necessary conditions for optimality of a constrained minimization problem in the calculus of variations, where the potential energy of the system is minimized subject to inequality constraints on displacements $\mathbf{u}(\mathbf{x})$ [15]. The contact stresses that appear explicitly in Eq. (4), assume the role of Lagrange multipliers associated with the inequality constraints on the displacements in such a *variational inequality* (VI) formulation. This problem can be solved using classical smooth optimization methods such as Sequential Quadratic Programming (SQP) and others. The VI formulation of the Signorini problem has the structure of a mixed complementarity problem (MCP), which has been widely researched in the mathematical programming community (see [16] for a review). Penalty methods, including variants such as the Augmented Lagrangian method and its modifications, have also been used to solve this problem [9]. Alternatively, the VI problem can be converted to a *variational equality* (VE) problem by assuming a specific contact boundary and treating contact stresses as additional variables.

Although all of the above techniques have been successfully used to solve the Signorini problem, none of these is directly suitable for use in an optimization framework. The sensitivity analysis in design problems involving unilateral contact conditions is complex and computationally expensive, when the contact interactions are modeled in the classical manner that leads to a VI formulation. Then, the computation of the sensitivity of the state variables with respect to the design variables requires the identification of active and semiactive constraints corresponding to that state [32,40]. This is difficult to do in an unambiguous manner for a problem with a large number of contact constraints due to the use of numerical optimization procedures. The penalty method requires a tradeoff between the desired accuracy of the state solution and ill-conditioning of the system of state equations. The Augmented Lagrangian and VE methods increase the size of the state vector by introducing additional variables.

The mathematical difficulties posed by the combinatorial (on/off) nature of contact interactions has prompted much recent work, which attempts to replace the complementarity conditions in Eq. (4) by a regularized approximation. Chen and Mangasarian [17] present a class of parametric *smoothing functions* that approximate the complementarity conditions by a continuously differentiable (smooth) functional and prove the existence of a solution to the reformulated MCP for arbitrary prescribed accuracy. Oden and Pires [18] had proposed regularization of the Coulomb friction law, which relates the tangential frictional force to the

normal reaction at the contact interface, to overcome the nondifferentiability inherent in the law at the onset of slipping. However, the use of regularization to smoothen the normal contact interaction has only been reported recently. Zavarise et al. [19] recently proposed a technique wherein a smooth functional is added to the potential energy expression to account for contact inequality constraints. This method, which they call *cross-constraint method* differs from the penalty methods in that it uses the smoothing functional to extend the constitutive relation between the contact pressure and the contact deformation into the no-contact range [20]. In the cross-constraint method the contact stiffness is a smooth function of the gap instead of being a constant as in the penalty based approach. The minimum of the unconstrained potential, which is the sum of the original potential energy and the new functional, can be controlled by tuning some parameters to lie arbitrarily close to the solution of the original constrained optimization. Moreover, the smoothing functional can be chosen such that in the post-contact range, the functional can take the form of an experimentally validated tribological constitutive law based on microscopic characterization of the contacting surfaces. Thus, this approach to regularization of the normal contact interaction can be considered an extension of a physics based constitutive contact model.

The approach taken in the present paper is similar to the cross-constraint method in principle but was derived independently from a different perspective as explained in Section 4. The regularization functional used in the work presented in this paper, is different from the one used by Zavarise et al. [19] and is chosen for the advantages which it brings to the solution of the design problem. In order to appreciate the need for a regularized contact model in design, the past work on optimal design involving elastic contact is described next with an emphasis on work related to structural optimization.

3.2. Structural design involving contact

The problem of optimal design involving contact arises in many practical applications such as fasteners (e.g., a rivet in [21]), machinery (e.g., engine poppet valve in [22], turbine blade-rotor connections in [23], die design in [24]), bridge supports etc. The last example falls under the purview of structural optimization, which deals with the optimal design of structures to sustain loads in the most efficient manner. Compliant mechanisms differ from structures in that, unlike structures, they are designed to transmit both force and motion [25]. Therefore, CMs need to be designed for stiffness to enable transmission of force and flexibility to enable transmission of motion. Despite the fundamental difference in objectives and their mathematical properties, topology optimization for design of CMs uses the same set of tools as structural optimization. Hence, the work done on optimal design of structures involving contact interactions is directly relevant to the work presented in this paper. Hilding et al. [8] recently reviewed the topic of structural optimization under unilateral contact and presented the past work in a unified way. In the rest of this section, we will adapt their notation to present the past work and relate it to the work done in this paper.

In most of the design problems involving contact, the objective and constraint expressions depend on the variables like displacements and stresses that characterize the state of the elastic body undergoing deformation. Let $\mathbf{s}$ denote the vector of variables that define the state of the system and $\mathbf{d}$ the design variables. The design variables determine the geometry (shape and topology of the elastic body, relative pose of the bodies that come into contact) and/or material properties, which in turn determine the stiffness of the system. A typical design problem can be written as

$$\begin{aligned} &\underset{\mathbf{d}}{\text{Minimize}} && \theta(\mathbf{s},\mathbf{d}) \\ &\text{subject to} && \mathbf{s} \in Z(\mathbf{d}), \\ &&& (\mathbf{d},\mathbf{s}) \in T, \end{aligned} \tag{5}$$

where Z indicates equations that govern the equilibrium state of the system. The set constraint T comprises the constraints related to contact as well as side constraints on the design variables. As Hilding et al. [8] note, nondifferentiability can arise in either the $\mathbf{d} \to \mathbf{s}$ mapping and/or in the $\mathbf{s} \to \theta$ mapping. Certain objectives are nonsmooth functions of the state variables making $\mathbf{s} \to \theta$ nondifferentiable. In the context of optimal design of elastic bodies in contact, the objective of minimizing the maximum contact stress over the contact boundary of the body (i.e., L^∞ norm of the contact stress) is one such example. This type of nondifferentiability can be readily avoided by using an energy-like norm (e.g., L^2 norm) instead of the L^∞ norm and reformulating the problem [26,27]. However, the nondifferentiability in the $\mathbf{d} \to \mathbf{s}$ mapping caused by the complementarity condition in Eq. (4) is difficult to eliminate. It occurs at *irregular points* in the design domain, at which both the gap and contact stress are simultaneously zero under some loading. This is a degenerate case, where the two bodies 'just touch' each other without transmitting any force across the contact interface. Intuitively, this nominal occurrence of contact with zero contact force can be associated with the point at which the transition between the two governing BVPs happens. The Karush–Kuhn–Tucker (KKT) necessary conditions for a minimum are not applicable at such irregular points, as they do not obey the *constraint qualification* needed by KKT conditions. This has a serious consequence when clas-

sical smooth optimization algorithms that look for a KKT point are used. If the minimum lies at an irregular point, these algorithms will not be able to find it. Even when the minimum does not lie at an irregular point, the smooth algorithms are usually not likely to find a minimum if they cannot easily *jump* over the irregular regions. Klarbring and Rönqvist [10] point out that the algorithmic difficulty associated with optimal structural design involving contact interactions arises from the ability of the contact force to vary significantly across two iterations even when the corresponding change in the design variables is very small. This is attributed to the sudden change in the boundary conditions at the onset of contact and leads to oscillatory behavior of the optimization algorithm, which in turn leads to lack of convergence for smooth optimization algorithms. Hilding [28] notes that unilateral contact constraints introduce a number of additional stationary points into the design domain, which hamper the ability of the optimization methods to locate the global minimum.

In problems related to minimizing the maximum contact reaction when the gap (or equivalently, the shape of the rigid surface) is chosen to be the design variable, Benedict and Taylor [26] showed that the optimization problem could be reformulated as minimization of the total equilibrium potential energy. Then, the optimization problem becomes differentiable and convex and therefore, can be solved by smooth optimization algorithms [8]. Techniques such as saddle point formulations [27], adaptation of smooth algorithms [11], and heuristic methods [21,29] have been shown to work in specific cases. However, the theoretically correct approach for solving nonsmooth optimization problems involves the use of nonsmooth optimization techniques, which use the more general concept of a subgradient instead of the usual gradient [30]. Stavroulakis [31] compared the behavior of two nonsmooth optimization algorithms (subgradient method and Bundle Trust-region (BT) method) and a heuristic adaptation of a smooth optimization algorithm to determine the optimal pre-stress force for stabilization of cracked masonry structures. He reported that the heuristic approach was unreliable, while the BT had the best overall performance. Outrata and Zowe [32] also used the BT algorithm to solve optimization problems with VI constraints.

However, due to the additional computational complexity associated with calculation of subgradients, these methods are not efficient for problems with a large number of design variables and many potential contact interactions, as is the case with the problem addressed in this paper. It is therefore not surprising that researchers in mathematical programming and structural optimization have sought to smoothen these problems in order to enable the use of robust and efficient smooth optimization techniques. Tin-Loi [33] and Hilding [28] used a heuristic smoothing procedure based on results of Facchinei et al. [34] to replace the unilateral contact constraints by a smooth parametric approximation. Both these papers re-solve the structural design problems solved by Klarbring and Rönqvist [10] using the smoothing procedure and smooth optimization algorithms. Hilding [28] also proves that under the assumptions of structural stability for the elastic body and linear independence of the contact constraints, a unique solution exists for the parameterized smoothened problem, which approaches the solution to the original problem asymptotically.

Almost all of the existing literature on structural design involving contact is limited to stiffness or strength related objectives. The only known exception known to the authors is the work of Kim et al. [35], who used the penalty method for shape optimization of a wind-shield wiper for a number of objectives that included force and motion transmission requirements. As mentioned earlier, in contrast to structures that are designed for maximum stiffness, flexibility is an essential aspect of the functionality of compliant mechanisms. It is known that simultaneous consideration of flexibility and stiffness makes this problem considerably different from stiffness optimization, and that this problem is nonconvex even in simple cases [36,37]. In order to circumvent the additional difficulties associated with the unilateral contact constraints, a technique for smoothing or *regularizing* the contact condition is proposed in this paper. It is called 'regularization' because its objective is to remove the irregular points caused by nondifferentiable $\mathbf{d} \rightarrow \mathbf{s}$ mapping. In conjunction with an associated concept of *state continuation*, this technique makes it possible to develop a practically feasible formulation for the design of CCMs. These features are described further in the next section.

4. Regularized contact model and state continuation

Incorporating a very stiff spring at the degrees of freedom where the displacements are specified is used in the *penalty* approach to imposing boundary conditions in finite element analysis [38]. The essential (or Dirichlet) displacement boundary condition is a *bilateral* constraint on the nodal displacement, since it eliminate the corresponding nodal degree of freedom completely. Consider a point on a structure, which undergoes a known displacement of h in the vertical direction as shown in Fig. 5a. A spring of high stiffness (C) and an artificial external force (F) can be used to model the essential displacement boundary conditions at the corner, as shown in Fig. 5b, without having to eliminate the corresponding fixed degrees of freedom.

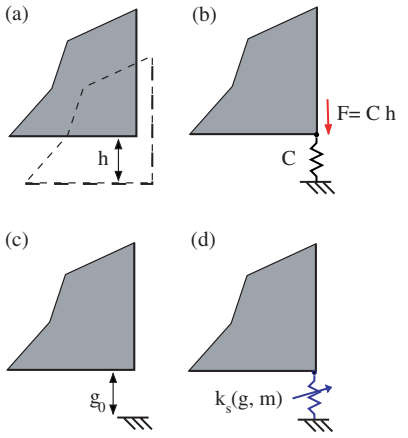

Fig. 5. A nonlinear spring can be used to model unilateral contact displacement boundary condition. Panels (a) and (b) show the penalty approach to model specified displacement (h) boundary conditions at a node in FEM. Panels (c) and (d) show how that idea can be extended to model unilateral contact boundary conditions using a nonlinear spring.

Intermittent contact at a point on the boundary of an elastic body is a displacement boundary condition that becomes effective when the gap between this point and a potential contact surface closes during the deformation under the action of applied loads (see Fig. 5c). In other words, the displacement constraint corresponding to a contact interaction is *unilateral* as it allows free movement of the node until the gap is closed. Therefore, a spring whose stiffness suddenly changes from a zero value before contact to a large value after the contact could model a contact boundary condition in a manner analogous to the spring enabled enforcement of essential displacement boundary conditions (see Fig. 5c, d). This is the physical interpretation of the penalty method used to solve the contact VI problem. Here, the stiffness of the spring varies as a *step function* of the gap corresponding to a point on the potential contact boundary of the body. While the use of a step function for the spring stiffness captures the enforcement of the unilateral displacement boundary conditions associated with the contact, it does not eliminate the mathematical and algorithmic difficulties associated with the complementarity conditions of Eq. (4). Approximating the step function by a smooth function such as a sigmoid helps alleviate some of these difficulties. The Hopfield neuron transfer function from neural networks is chosen as the sigmoid function because it is a single parameter generalization of the step function that approaches its bounds asymptotically and without an overshoot.

Consider a hypothetical nonlinear spring attached between a potential contacting point on the body and a corresponding point on the rigid surface (see Fig. 6a). The stiffness (k_s) of this hypothetical spring used to implement regularized contact, can be expressed in terms of the nodal displacement x, initial gap g_0, a large post-contact stiffness γ, and a sharpness parameter m as:

$$k_s = \frac{\gamma}{1 + e^{-m\left(\frac{x}{g_0} - 1\right)}}. \tag{6}$$

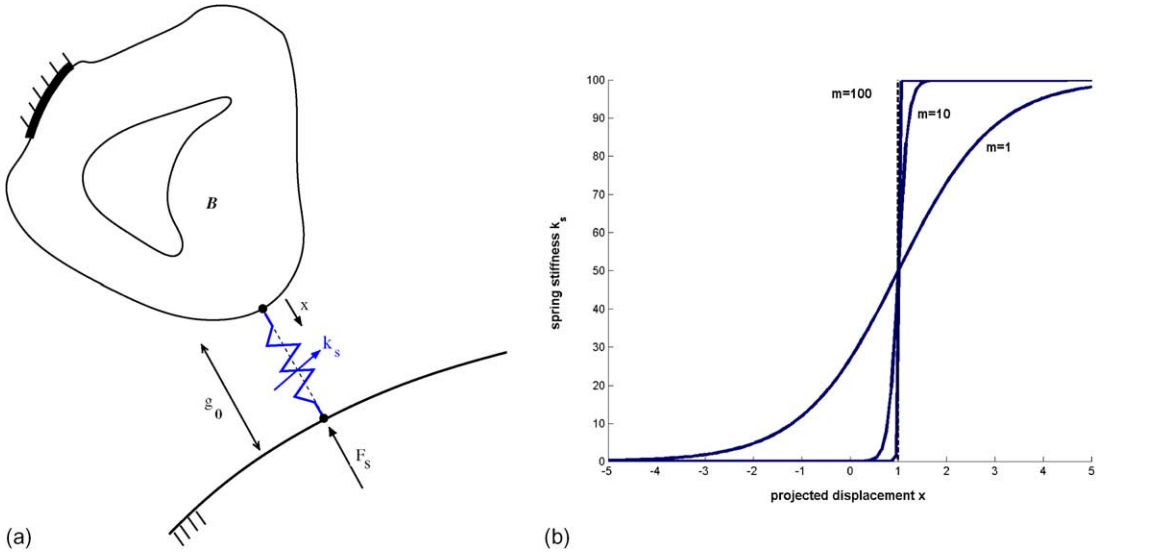

Fig. 6. Smoothened modeling of contact for small deflections: (a) a nonlinear spring with variable stiffness models the contact, (b) parametric regularized contact stiffness function.

The interpretation of the regularized contact model in terms of a nonlinear spring makes this model very similar to the *action-at-a-distance* contact model of Zavarise et al. [19].

The nodal displacement x at any point is the projection of the displacement of that point along the axis of the spring. In reference to Fig. 4, x represents $-u_n$. The axis of the spring, which is chosen at the outset to lie along the normal to the contact surface, indicates the line of action of the contact force under the assumption of small deformations. The contact reaction is modeled by the force in the hypothetical contact spring. The sharpness parameter m, controls the sharpness of the transition from pre- to post-contact and can take any positive real value. A plot of $k_s(x, m)$ for $\gamma = 100$ and $g_0 = 1$ can be seen in Fig. 6b for three different values of m. When $m \to \infty$, the stiffness function approaches a step function as desired, giving a contact stiffness of γ as soon as the gap is fully closed. For smaller values of m, the stiffness is spread out over the gap and is nonzero even when the gap is not closed. It is important to note that for any value of m, the contact is *always on*, and more importantly, the sharpness of the transition from pre- to post-contact can be controlled by varying m. The nondifferentiability associated with the complementarity conditions in Eq. (4) is circumvented as the contact reaction, now has a uniquely defined gradient for all permissible values of m.

It is clear that the modeling of contact interaction in the above manner is consistent with the mechanics of contact only for high values of m. Numerical experiments show that $m = 50$ gives a very close approximation and $m = 500$ is indistinguishable from a step function. The significance of this approach to modeling contact lies in the fact that a single real-valued parameter (m) can be used to generate a sequence of BVPs, which converges to the Signorini BVP as $m \to \infty$, although that limit is quite unnecessary in practical problems. The mathematical properties of this function and the convergence behavior of Newton-type optimization algorithms for regularized formulations of MCPs using this function are discussed in detail by Chen and Mangasarian [17]. These properties can be used to advantage during optimization, by splitting the single optimization problem into a sequence of sub-problems corresponding to monotonically increasing values of m. A small value for m is used in the beginning of the optimization process along with a uniform starting guess. This results in a smooth or differentiable problem that can be readily tackled by gradient-based smooth optimization algorithms. The optimal design resulting from this sub-problem is then used as the starting guess for the next sub-problem together with a larger value for m. This process is continued until a reasonably high value of m is reached, which guarantees that the final design is consistent with the mechanics of contact for the problem. Since only small deflections are considered in this paper, the direction of the spring force, which models the contact force, can be assumed to remain constant. The sequence of BVPs generated by gradually increasing the single real-valued parameter (m) defines a sequence of approximations to the actual state BVP. Following Ortega and Rheinboldt [39], the sequential optimization approach described above will, therefore, be referred to as state *continuation* in the rest of this paper.

It should be noted that the state continuation approach is not necessary for obtaining the state solution, i.e. the regularized state problem can be solved directly for any permissible value of the sharpness parameter. The reader is referred to Chen and Mangasarian [17] for proofs of the existence and uniqueness of a solution to the regularized problem for any permissible m. However it is more advantageous to use the state continuation approach for the optimization-based design problem as this brings an additional algorithmic advantage. This can be explained in an intuitive manner as follows. Since contact is 'always on', there is a small but finite 'contact reaction' even before the gap is closed. This serves as an indication of the impending contact to the optimization algorithm. The algorithm can then explore the use of contact, if the contact is found to be useful in furthering its aim of minimizing the objective or satisfying the constraints. As sequential optimization progresses, the value of m is increased and hence potential contact points that are far from their respective rigid surfaces do not experience significant forces (see Fig. 6b) from the hypothetical contact spring. So, only those points that the algorithm chooses to involve in contact will be effective at the later stages of optimization. Consequently, if contact springs are defined at all points along the boundary of the design region, which are not used for any other purpose, the algorithm can choose where contact should take place. Choice of an appropriate initial value of m and the rate at which it is increased depends on the problem and is discussed in Section 7 in the context of design examples. The design problem for synthesizing CCMs to meet desired specifications using this approach is described next.

5. Formulation of the CCM synthesis problem

Intermittent contact introduces sufficient nonlinearity into the system, to yield CCMs with prescribed force–deflection (F–δ) curves and output paths even with small deflections. More importantly, the behavior can be nonsmooth, which is a unique characteristic of CCMs. As is common in path generation problems, the desired response is specified by a number of *precision* points, each of which comprises a value of the input

force and the value of the response desired at that force [12,13]. The circles in Fig. 7 show desired nonlinear and nonsmooth force–deflection specifications. These are compared with analogous points (dots in Fig. 7) generated by a candidate design. Least squares error between the desired and designed curve, as measured at the precision points, is the objective function to be minimized.

In this paper, a beam ground structure (i.e., a network of nonoverlapping beam elements) is used to parameterize the design domain for topology optimization. All elements have the same out-of-plane thickness to facilitate ease of fabrication at the macro and micro scales. The widths (**w**) of the elements in the design domain and the initial gaps (**g**) at the potential contact nodes are treated as design variables. The design variables are bounded by side constraints that are governed by numerical or manufacturing considerations. If a design element's width goes to its lower bound w_{lb}, which that is chosen to be a very small positive value, then that element is said to have reached a *nonexisting* state and is considered absent from the final design. Thus, the elements that are deemed to 'exist' in the design define the topology of the design. Any of the nodes on the boundary of the design region can be considered potential contact nodes except when they have specified displacements or applied loads. Since the problem is known to be nonconvex, a volume constraint is imposed to explore different regions of the design domain. The optimization problem can now be posed as follows:

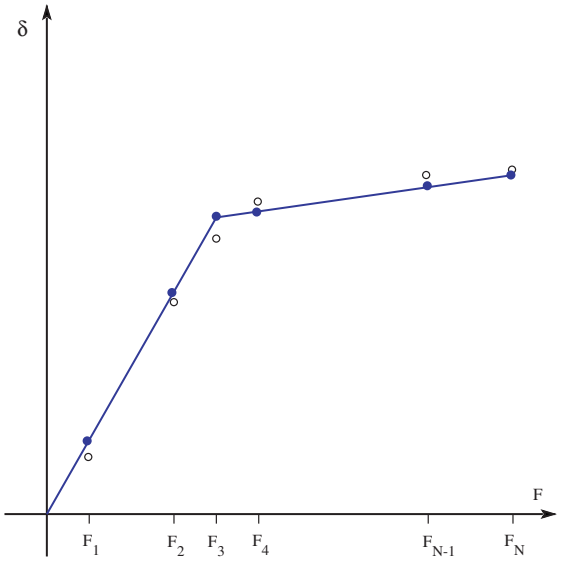

Fig. 7. Nonsmooth response specification for CCMs synthesis. The circles indicate the design data points, while the dots indicate the response of an actual trial mechanism.

$$\begin{aligned} &\underset{\mathbf{d}}{\mathrm{Min}}\theta = \sum_{\mathrm{i}=1}^{\mathrm{N}} \left(\delta_{\mathrm{i}} - \delta_{\mathrm{i}}^{*}\right)^{2} \\ &\text{subject to} \quad \text{static equilibrium equations} \\ &\text{given :} \quad \text{geometry of the input region,} \\ &\qquad\qquad \text{boundary conditions,} \\ &\qquad\qquad \text{input force,} \\ &\qquad\qquad \text{potential contact nodes,} \\ &\qquad\qquad \text{smoothening parameters and} \\ &\qquad\qquad \text{material properties,} \end{aligned} \tag{7}$$

where N is the number of precision points, $\mathbf{d} = (\mathbf{w}, \mathbf{g})$ is the vector of design variables, δ_i is the actual response measure and δ_i^* is the specified response value corresponding to the ith precision point. While path and $(F–\delta)$ objectives highlight the most significant enhancement of the capabilities of compliant mechanisms by CCMs, they can also be designed for other objectives and multiple load cases. This will be discussed further in the context of design examples in Section 7. The analytical computation of the gradients of the objective and constraints with respect to **d** is discussed next.

6. Sensitivity analysis and solution method

The regularized contact model described in Section 4 makes the computation of the state sensitivities straightforward and efficient by using a continuously differentiable approximation of the contact constraints. Only the gradient of the displacement vector ($\mathbf{u} \in \mathbf{s}$) is computed below as the sensitivities of all other state variables and the objective can be computed from it.

At equilibrium, for the reduced system (i.e., after applying the essential displacement boundary conditions), in discretized (finite element) notation, we have

$$\mathbf{F}_{\mathrm{int}} + \mathbf{F}_{\mathrm{s}} = \mathbf{F}_{\mathrm{ext}}, \tag{8}$$

where $\mathbf{F}_{\mathrm{int}}$ is the internal force, $\mathbf{F}_{\mathrm{ext}}$ is the applied external force, and $\mathbf{F}_{\mathrm{s}}$ is the contact reaction. The internal force is given by $\mathbf{F}_{\mathrm{int}} = \mathbf{K}\mathbf{u}$, where $\mathbf{K}$ is the stiffness matrix corresponding to the elastic design domain and $\mathbf{u}$ is the displacement vector. The contact reaction is modeled by the force in the hypothetical contact springs at all degrees of freedom that are defined to be potential contact locations. The magnitude of the spring force F_{s}^{j} at jth node can be computed by integrating the spring stiffness from Eq. (6) because $k_{\mathrm{s}}^{j} = (\mathrm{d}F_{\mathrm{s}}^{j}/\mathrm{d}x_j)$. Thus,

$$F_{\mathrm{s}}^{j} = \int_{0}^{x_j} k_{\mathrm{s}}^{j}\,\mathrm{d}x = \frac{\gamma g_0^{j}}{m} \ln\left[\mathrm{e}^{m\left(\frac{x_j}{g_0^{j}}-1\right)} + 1\right], \tag{9}$$

where x_j is the projected displacement of the node along the axis of the contact spring and g_0^j is the initial gap at

node j. It should be noted that although linear elastic material behavior and small displacements are assumed, Eq. (8) is nonlinear because of the presence of the $\mathbf{F}_s$, which depends on the displacement ($\mathbf{u}$). Hence, it is solved by accumulating small external load increments and using Newton–Raphson iterations to restore equilibrium at every increment [41]. The incremental (*predictor*) and iterative (*corrector*) equations are respectively given as

$$\begin{aligned} \mathbf{K}_e \Delta \mathbf{u} &= \Delta \mathbf{F}_e, \\ \mathbf{K}_e \delta \mathbf{u} &= -\mathbf{r}, \end{aligned} \tag{10}$$

where $\mathbf{K}_s = \mathrm{d}\mathbf{F}_s/\mathrm{d}\mathbf{u}$ can be interpreted as the *contact stiffness* matrix, $\mathbf{K}_e$ $(= \mathbf{K} + \mathbf{K}_s)$ is the effective stiffness matrix, $\mathbf{r}$ $(= \mathbf{K}\mathbf{u} - \mathbf{F}_s - \mathbf{F}_e)$ is the force residual, $\Delta\mathbf{F}$ is the external load increment, $\Delta\mathbf{u}$ is the corresponding predictor solution and $\delta\mathbf{u}$ is the corrector term.

Noting the following functional dependencies: $\mathbf{K}(\mathbf{w})$, $\mathbf{u}(\mathbf{d})$ and $\mathbf{F}_s(\mathbf{u}, \mathbf{g})$, Eq. (8) can be differentiated with respect to the design variable to yield

$$\begin{aligned} &\left(\mathbf{K} + \frac{\mathrm{d}\mathbf{F}_s}{\mathrm{d}\mathbf{u}}\right)\frac{\mathrm{d}\mathbf{u}}{\mathrm{d}\mathbf{d}} = -\left(\frac{\mathrm{d}\mathbf{K}}{\mathrm{d}\mathbf{w}}\mathbf{u} + \frac{\mathrm{d}\mathbf{F}_s}{\mathrm{d}\mathbf{g}}\right), \\ &\therefore \quad \mathbf{K}_e\frac{\mathrm{d}\mathbf{u}}{\mathrm{d}\mathbf{d}} = -\left(\frac{\mathrm{d}\mathbf{K}}{\mathrm{d}\mathbf{w}}\mathbf{u} + \frac{\mathrm{d}\mathbf{F}_s}{\mathrm{d}\mathbf{g}}\right). \end{aligned} \tag{11}$$

In deriving Eq. (11), we used the fact that the external force does not depend on either the design variable or the displacements. While Eq. (11) is written to emphasize the structure of the sensitivity relation, in the actual implementation the terms in it need to be resized to fit the dimension of $\mathbf{d}$. The above equation is similar to the incremental equilibrium equation (Eq. (10)), therefore, the factorization of the effective stiffness matrix for the sensitivity analysis in (Eq. (11)) is already available as part of the equilibrium analysis. The right hand side vector can be obtained readily from Eqs. (6) and (9). Since sensitivities are needed at every precision point in the specified response (Eq. (11)) needs to be solved for every load step that corresponds to a precision point in the desired response.

Having obtained the sensitivities without much computation beyond the state evaluation, it is now easy to apply a gradient-based smooth optimization algorithm to solve the optimization problem in (Eq. (7)). The example problems presented in the next section were solved using `fmincon` function in Matlab's *Optimization Toolbox*. This routine combines Sequential Quadratic Programming (SQP) and trust region algorithms. A line search, performed by a combination of golden section method and quadratic approximation, can be optionally used at every iteration to make the solution procedure robust.

7. Examples

This section presents four examples of CCMs that are synthesized using the approach outlined in Section 4.

7.1. Mechanical OR gate

Mechanical implementations of logic gates, which are the basic building blocks of digital computation, have attracted renewed interest in the wake of increasing sophistication achieved by microfabrication processes and the need for radiation-resistant secure computing resources. Bergstrom et al. [42] report the design and fabrication of a complete family of micromechanical logic elements that uses a sliding micromechanical contact actuated by an electrostatic motor. Since, the device function depends on relative sliding between two components, they note that the speed of device operation is limited by frictional heating. The first design example addresses the synthesis of a CCM that behaves like a mechanical OR gate. Unlike the design reported by Bergstrom et al., this design uses minimal sliding and hence, is less constrained by frictional heating.

The design specifications are shown schematically in Fig. 8. The square design domain is parameterized by four cells, each of which is defined by eight beam elements that connect four corner nodes and a central one. The design domain is shown as the shaded square in the figure, while the ground structure that parameterizes the domain is overlaid in black lines. The bottom left node (marked by E) and the bottom right node are fixed to the ground, i.e. the x, y and slope degrees of freedom are constrained to be zero. The two input ports correspond to the nodes at which, the externally applied loads (F_1 and F_2) are shown to act. The output port is at the top center node and has a spring (W) attached to it, which is compressed to register a positive output. Potential contact surfaces are indicated by C_i, $i = 1, 2, 3$. All boundary nodes that are not associated with a fixed boundary condition, an applied force or the output port, are

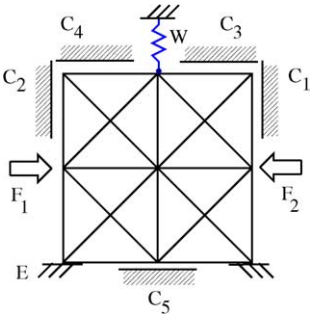

Fig. 8. Schematic of the problem specification for the synthesis of a mechanical OR gate.

considered as potential contact nodes. As an example, the top left node is a potential contact node, which may contact one or both of the rigid surfaces marked C_2 and C_4. A small positive numerical value is chosen as the lower bound for the design variables to avoid numerical ill-conditioning problems. The data used for the problem are summarized in Table 1 below. The starting value for the sharpness parameter (m_0) is chosen such that the contact force at any contact node, in the absence of any external load, is approximately 0.5–1% of the applied force magnitude (e.g. $F_1 = F_2 = 150$ N for this example). This ensures that a small but nonzero contact reaction exists from the outset. On the successful convergence of a step of the sequential optimization process for a given m, the sharpness parameter is increased by $\Delta m = 15\%$ for the next step. This is repeated until the sharpness parameter exceeds m_f ($=200$). These heuristic rules for the choice of m_0, Δm and m_f are based on numerical experiments and will be used for all the problems considered in this paper.

The objective to be maximized is defined as:

$$\max_{\mathbf{d}} \theta = \mathbf{Z}(\mathbf{f_1} \cdot \mathbf{f_2}), \tag{12}$$

where Z is a scaling factor and $f_i = (\delta/\mathrm{SE})_i$ is the ratio of the displacement at the output port (δ) to the corresponding strain energy (SE) stored in the elastic body only, for the ith load case. The motion transmission requirement is represented by δ, while $1/\mathrm{SE}$ ensures adequate stiffness in the mechanism to enable load transmission. Therefore, maximizing f_i is a convenient objective for designing a compliant mechanism for the ith load case [25]. Load case 1 corresponds to the case when *only* the external load F_1 is applied, while load case 2 corresponds to when *only* load F_2 is applied. Taking the overall objective as the product of the individual load case objectives ensures that the optimization algorithm seeks a design satisfies both load cases. Then, symmetry of the problem dictates that the combination of these load cases also be satisfied by the design. The *truth table* summarizing the behavior of an OR gate and the corresponding load cases for this problem is given below in Table 2.

Table 1
Numerical data for the mechanical OR gate example

Width lower bound	w_{lb} [mm]	0.08
Width upper bound	w_{ub} [mm]	10.0
Gap lower bound	g_{lb} [mm]	0.001
Gap upper bound	g_{ub} [mm]	80.0
Thickness	t [mm]	3.175
Young's modulus	E [N/mm^2]	1312.0
Width starting guess	$\mathbf{w}_0$	25%
Volume constraint	V^*	50%
Gap starting guess	g_0	6.25%
Starting sharpness parameter	m_0	11.3
Post-contact stiffness	γ [N/mm]	1.0E+05
Output spring stiffness	k_w [N/mm]	10.4

The solution obtained from the synthesis procedure is shown in Fig. 9, while Fig. 10a–d show a polypropylene prototype of the design actuated by the different load cases from Table 2. The dark lines in Fig. 9 represent widths in the final design normalized by w_{ub}. The dotted lines represent elements that have reached their lower bound and are deemed absent from the final design. The values of the initial gaps obtained for the solution are given as $g_{C_1} = 0.0012$, $g_{C_2} = 0.001$, $g_{C_3} = 0.658$, $g_{C_4} = 0.660$ and $g_{C_5} = 0.001$ mm. It is observed that the design uses very small initial gaps at the vertical contact surfaces in C_1 and C_2, as well as at the horizontal contact surface at C_5. These can be interpreted as roller supports in the physical realization of the design. Two segments at the center of the design in Fig. 9 are absent from the prototype as they were too thin to be manufactured at this scale. The device is mounted in a pocket machined in Plexiglas, such that the walls of the pocket provide the necessary contact surfaces. For clarity, the relevant contact surfaces are overlaid with solid lines in the pictures.

The convergence history for the objective function across steps in the sequential optimization process is

Table 2
Truth table of the OR gate

Input 1	Input 2	Output	External load
0	0	0	–
0	1	1	F_2
1	0	1	F_1
1	1	1	F_1, F_2

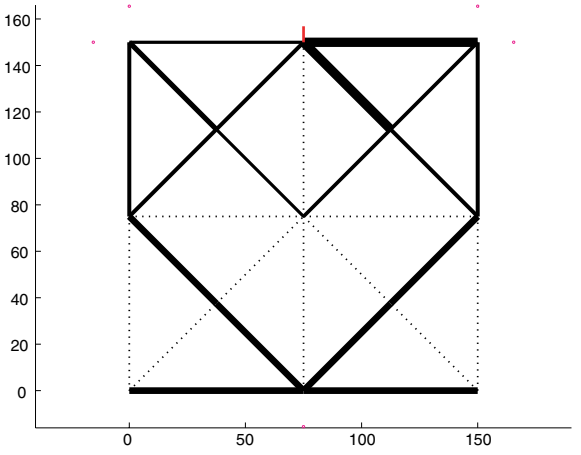

Fig. 9. The design for a mechanical OR gate obtained from the solution procedure. The axes are marked in mm.

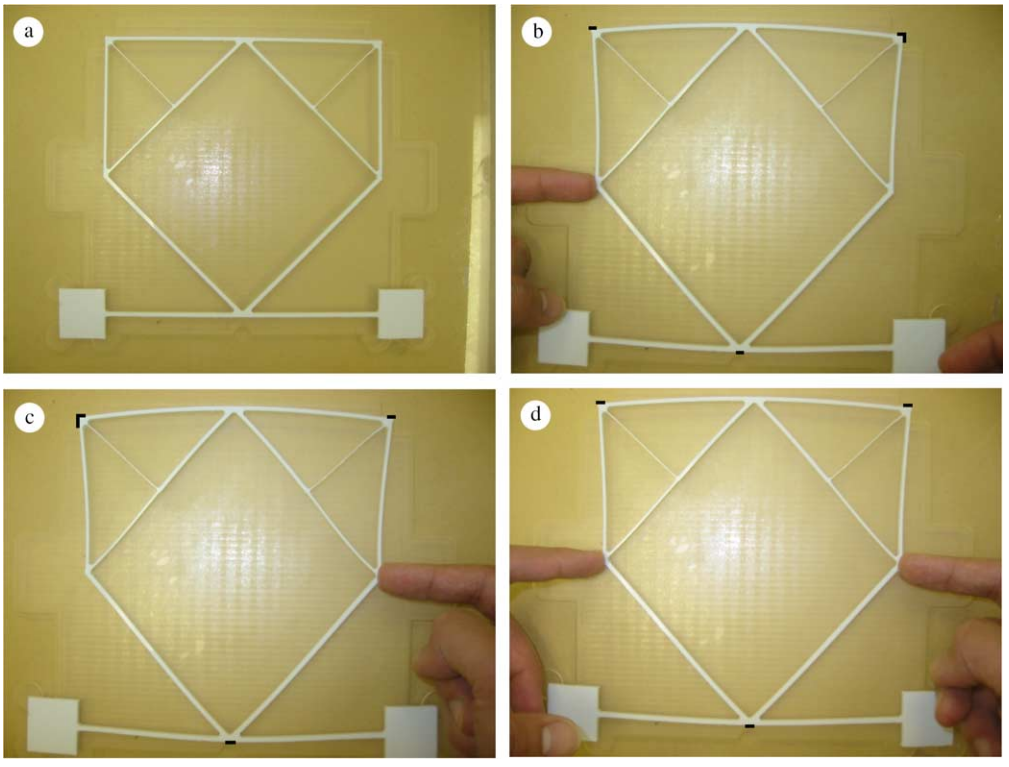

Fig. 10. A prototype of the symmetric design milled from polypropylene is shown in (a). The deformed configurations under load cases 1, 2 and 1 + 2 are shown in (b)–(d) respectively.

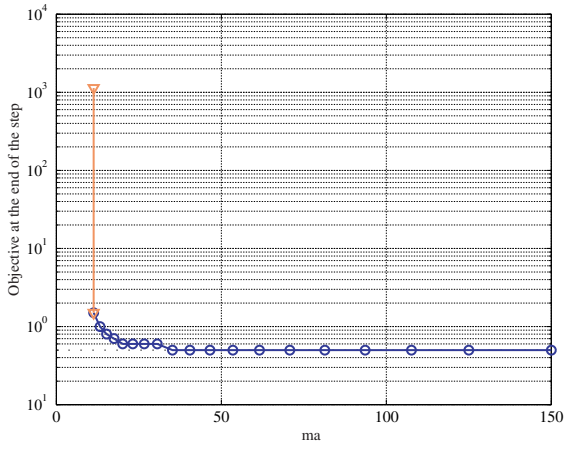

Fig. 11. The convergence history for the OR gate example.

shown in Fig. 11. [1] The light gray curve with triangle markers represents the improvement in the first step starting with the uniform initial guess. The solid black curve with hollow dot markers (blue) indicates the progress of the sequential optimization process across increasing values for the sharpness parameter (m). Note that, the maximization problem in Eq. (12) is equivalently formulated as minimize $-\theta$, which is the form used for this problem.

The path of the output port of the final OR gate design (i.e. after removing all 'disappeared' elements) for different load conditions as predicted by nonlinear FEA using ABAQUS© is shown in Fig. 12. All curves in the right half-plane correspond to load case 1 ($F_1 = 300$ N), those in the left half-plane correspond to load case 2 ($F_2 = 300$ N), while those in the center correspond to *both* F_1 and F_2 ($= 150$ N) acting simultaneously. The solid dark gray curves without any markers (red in the electronic version) correspond to the final design. These curves together with the prototype performance from Fig. 10a–d demonstrate that the design behaves like a logical OR gate.

The design in Fig. 9 is slightly asymmetric even though the problem formulation appears to be symmetric. The influence of this asymmetry on device response can be seen in a small difference between the maximum Y displacement for load cases 1 and 2 in Fig. 12. It is also instructive to compare the performance of the asymmetric final design with that of its symmetric

[1] For interpretation of color in Figs. 2, 3, 5–13, 15–19, 21–26, the reader is referred to the web version of this article.

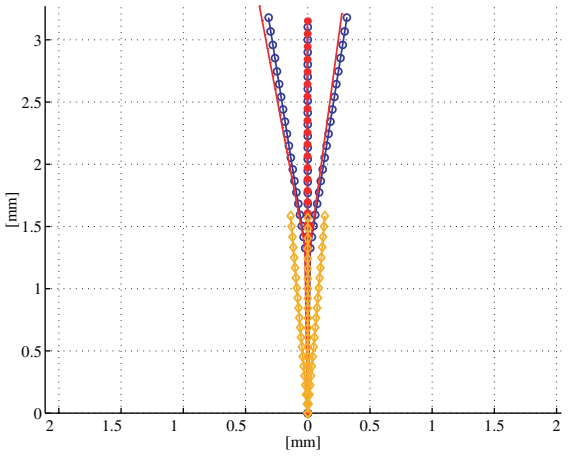

Fig. 12. The path of the output port of the OR gate design for different load conditions as predicted by nonlinear FEA using ABAQUS©.

version (solid black line with circles in Fig. 11, blue in the electronic version). The symmetric version is obtained by using the mean widths of corresponding elements as the common width for both elements. It is seen that the symmetric version gives equal final Y displacements for load cases 1 and 2, but this value is less than the max Y displacement (load case 2) for the asymmetric design. Therefore, it is clear that the objective in Eq. (12) is minimized by a slightly asymmetric design. The origin of this asymmetry is not clear and probably can be attributed to numerical artifacts.

Since the response for each individual load case is smooth, is contact really needed to meet this design specification? As the final values for the initial gaps are small, it is instructive to analyze the behavior of the final design by replacing all contacts with fixed boundary conditions (i.e. x, y and slope, all constrained to be zero). The resulting output path is also plotted in Fig. 12 in light gray solid lines with diamonds (gold). Although the basic nature of an OR gate is retained, the corresponding deflections are much smaller. It is also noted that if all contact constraints are completely removed, the design behaves like a logical AND gate, whose topology differs from that presented by Saxena and Ananthasuresh [36].

7.2. "Grasp and pull" gripper

Unlike in rigid-body mechanisms, where the kinematics of operation can be studied independent of the kinetics, these two aspects of mechanism behavior are related by a constitutive law in CMs. Hence, the properties and orientation of the workpiece influence the optimal design of a CM designed to manipulate it [43,44]. When the stiffness of the workpiece is comparable to that of the mechanism, the standard practice of using a spring to model the workpiece, gives reasonable results. However, when the workpiece stiffness differs considerably from that of the mechanism, the use of a constant stiffness spring to model the workpiece makes the optimal synthesis problem ill-conditioned and thereby, results in sub-optimal designs. Bruns and Tortorelli [45] used a spring that was activated after a prescribed initial free travel of the CM output port. This enabled them to separate the low output stiffness pre-grasp motion from the relatively higher output stiffness post-grasp motion. The hypothetical nonlinear spring used to model smoothened contact in this work can readily model this behavior. The post-contact stiffness (γ) in Eq. (6) is chosen to be the stiffness of the workpiece, while the initial clearance between the output port and the workpiece is chosen as the initial gap (g_0). As the workpiece is not a design element, the initial gap is treated as constant.

The limited maneuverability and degradation of tactile feedback associated with laparoscopic surgical tools have prompted recent research into compact multifunctional surgical tools (e.g. [46]). This example presents a CCM gripper, which exploits the high stiffness of the workpiece to exhibit multifunctional behavior that can be used e.g. in a suturing procedure. Only one-half of the symmetric design is illustrated in the subsequent figures. The force–deflection objective formulation from Eq. (7) is used this problem. Again a uniform starting guess is used along with the parameters shown in Table 3 below. Since, very stiff workpieces are considered (e.g. a suture needle), the post-contact stiffness of the workpiece is assumed to be the same as that for a rigid external contact surface, although it can be chosen to be any finite value.

The schematic of the problem specification is shown in Fig. 13 following the same convention as in example 1. The output port is labeled O, the workpiece modeled by hypothetical nonlinear contact spring is labeled W, roller supports along the line of symmetry are marked R, and the desired output path is labeled P. All

Table 3
Numerical data for the grasp-and-pull gripper

Width lower bound	w_{lb} [mm]	0.08
Width upper bound	w_{ub} [mm]	10.0
Gap lower bound	δ^0_{lb} [mm]	0.001
Gap upper bound	δ^0_{ub} [mm]	50.0
Thickness	t [mm]	3.175
Young's modulus	E [N/mm^2]	1312.0
Width starting guess	$\mathbf{w}_0$	50%
Volume constraint	V^*	100%
Gap starting guess	g_0	21%
Starting sharpness parameter	m_0	10.0
Post-contact stiffness	γ [N/mm]	1.0E+05
Incrementation factor for m	Δm	15%

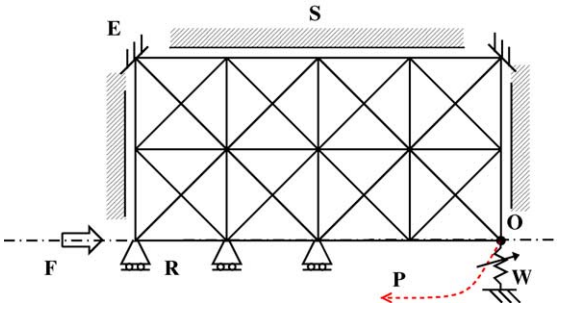

Fig. 13. Schematic of the problem specification for the synthesis of a grasp and pull gripper.

boundary nodes adjacent to an external surface that are otherwise unused, can contact that surface. The maximum applied force (F) is 200 N and the initial gap between the output port and the workpiece is closed after 3.352 mm of vertical travel.

The design obtained from the synthesis procedure is shown in Fig. 14. Only the nonlinear contact spring representing the workpiece in Fig. 13 is active in the final design. This is significant because it shows that the synthesis procedure uses contact only where it is necessary. In other words, the regularized contact model does not bias the procedure into selecting designs that necessarily use contact. Fig. 15 shows a polypropylene prototype of the design in its original and actuated configurations.

The performance of the actual device is compared with the design specifications in Fig. 16. The solid black curve with asterisks represents the actual force–

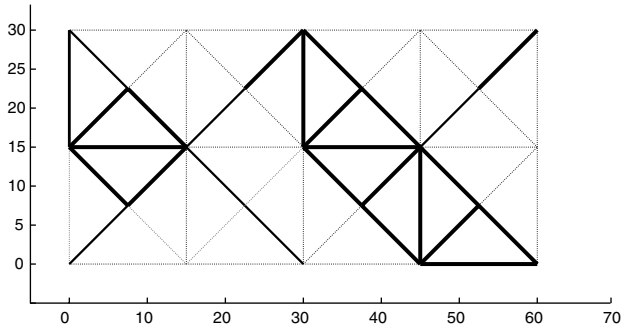

Fig. 14. The grasp and pull gripper design obtained from the solution procedure. The axes are marked in mm.

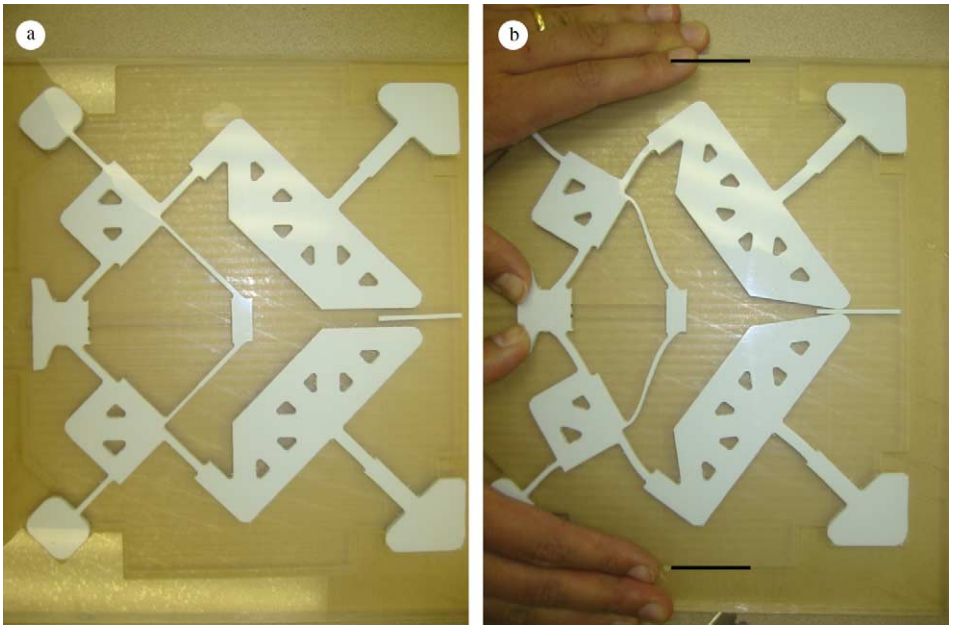

Fig. 15. A polypropylene prototype of the grasp and pull gripper design in its original (left) and deformed (right) configurations.

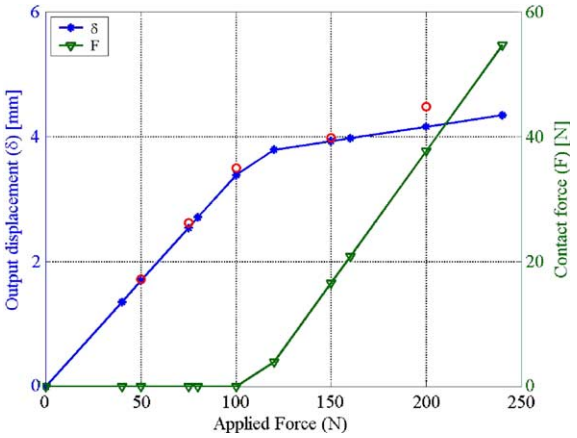

Fig. 16. Performance characteristics of the grasp and pull gripper.

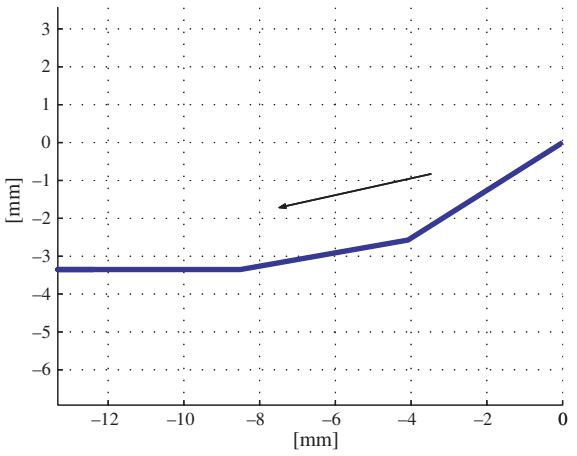

Fig. 18. The simulated path for the output port of the grasp and pull gripper obtained from nonlinear FEA using ABAQUS.

deflection characteristics of the final design. The specified characteristics are overlaid in circle markers. The contact representing interaction with the workpiece is the only active contact in the final design and the corresponding contact force represents the force exerted on the workpiece. To facilitate visualization of the pre- and post-contact phases of motion, the contact force is overlaid in the figure in a solid gray curve with triangles (green) to the scale shown at the right. The convergence history for this synthesis run is shown in Fig. 17, while the output path simulated for the final design using nonlinear FEA is shown in Fig. 18. It is interesting to note that the final design exploits the stiffness of the workpiece to exhibit a much higher post-contact stiffness that allows the mechanism to transmit a high output force. At the same time, the mechanism uses the separation of the pre- and post-contact phases to retain much lower output stiffness in the pre-contact stage, which enables a rapid and relatively free initial grasping motion.

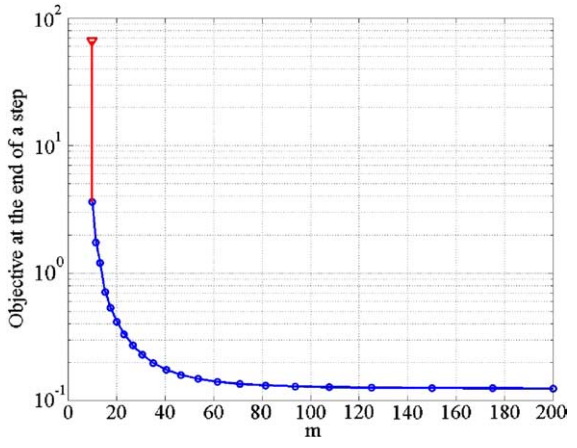

Fig. 17. Convergence history for the grasp and pull gripper.

7.3. Displacement delimited gripper

The ability to manipulate matter at the micrometer and nanometer length scales has opened new avenues for scientific enquiry. As assembling or manipulation tools of sufficient functionality at these length scales is infeasible, CMs are a natural choice for such tools. However, to date only relatively simple mechanical structures like a cantilever beam (e.g. in an atomic force microscope) have been used for studies in manipulating and characterizing very small fragments of matter (e.g. blood cells and carbon nanotubes). CMs, and CCMs in particular, can realize tools, which can not only be easily fabricated at the microscale but also offer functionality comparable to modern hand tools. In this example, a CCM gripper is designed to have its output port motion constrained by a specified maximum displacement in a given direction. In other words, once the specified component of the output port displacement reaches a preset limit, any further increase in the input force does not cause a change in that component of the output displacement. Such a gripper can be used to grasp soft and delicate workpieces without using complex feedback control to avoid damaging them.

A schematic of the problem specification is shown in Fig. 19 and the corresponding numerical data is listed in Table 4. Due to the symmetry of the problem, only one-half of the design domain is shown. As in example two, the workpiece is also modeled as a nonlinear spring but it is not a design variable. The workpiece stiffness is 5 N/mm and the maximum applied load (F) is 150 N.

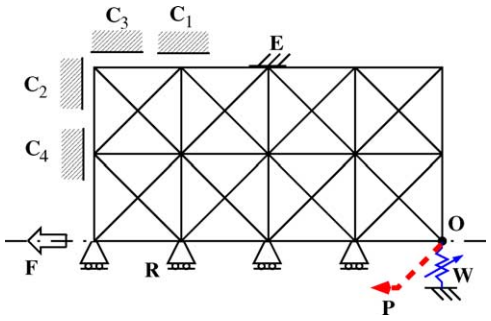

Fig. 19. Schematic of the problem specification for the synthesis of a displacement delimited gripper.

Table 4
Numerical data for the displacement delimited gripper

Width lower bound	w_{lb} [mm]	0.01
Width upper bound	w_{ub} [mm]	7.5
Gap lower bound	g_{lb} [mm]	0.001
Gap upper bound	g_{ub} [mm]	80.0
Thickness	t [mm]	3.175
Young's modulus	E [N/mm^2]	1312.0
Y displacement limit at the output port	[mm]	5
Width starting guess	$\mathbf{w}_0$	20%
Volume constraint	V^*	50%
Gap starting guess	g_0	50%
Starting sharpness parameter	m_0	12.0
Post-contact stiffness	γ [N/mm]	1.0E+05
Incrementation factor for m	Δm	15%
Constant output spring stiffness for load case 2	k_w [N/mm]	5.5

Unlike in example two, the objective in Eq. (7) cannot be used directly in this case as the workpiece stiffness is small. In order to avoid flimsy topologies that fulfill the design specifications but are unable to transmit force to the output port, the force–deflection objective in Eq. (7) is modified as below.

$$\underset{\mathbf{d}}{\text{Min}}\ \theta = \alpha\theta_{\mathbf{1}} + (\mathbf{1}-\alpha)\theta_{\mathbf{2}}, \tag{13}$$

where, θ_1 is given by Eq. (7), while θ_2 differs from θ_1 only in the addition of a constant stiffness spring at the output port. This spring should not be confused with the nonlinear spring used to model the workpiece. The weighting factor α ($=95\%$) is used to give precedence to the actual problem (θ_1) over the artificial one (θ_2), which is used only to obtain well-defined and robust designs. This is similar to the approach used by Pedersen et al. [13] for the synthesis of large deflection CMs. The parameters used in the procedure are summarized in the table below. The potential contact surfaces are chosen keeping the application in mind such that they lie at the base (left) end of the gripper and leave the gripping end free.

The design obtained from the optimization process is shown in Fig. 20 and a polypropylene prototype is shown in Fig. 21 in its original and actuated configurations. Only the contact C_1 from Fig. 19 is used by the final design. The performance of the design (solid black line, blue) is compared with the specified force–deflection relation (hollow gray dots, red) in Fig. 22. The variation in the magnitude of the contact reaction at C_1 is also overlaid in Fig. 22 in dark gray dotted curve (green) corresponding to the scale on the right.

The magnitude of the contact reaction becomes comparable to the applied load after the preset Y displacement limit of 5 mm is exceeded. This contact reaction counterbalances the influence of the applied load to constrain further motion of the output port. The convergence history for the optimization is shown in Fig. 23. Simulation of the final design using ABAQUS yields the path of the output port shown in Fig. 24 for a maximum input load of 200 N. The X and Y

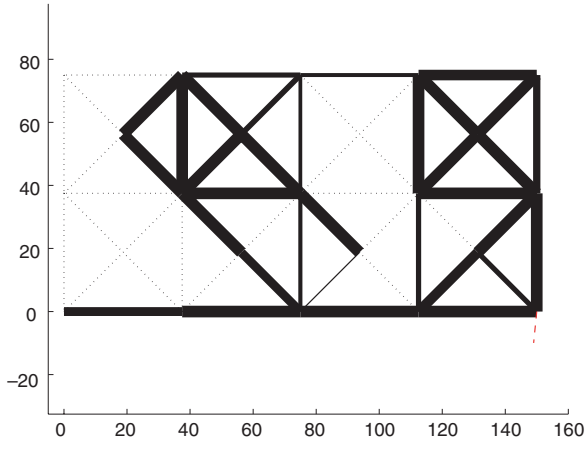

Fig. 20. The displacement delimited gripper design obtained from the sequential optimization procedure. The axes are marked in mm.

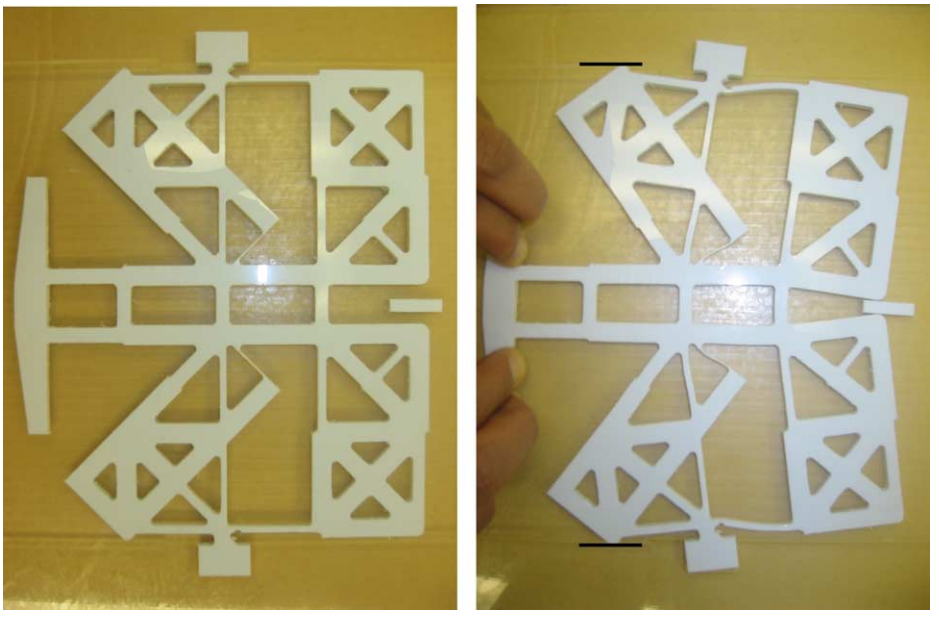

Fig. 21. A polypropylene prototype is shown in the original configuration (left) and in the actuated configuration (right).

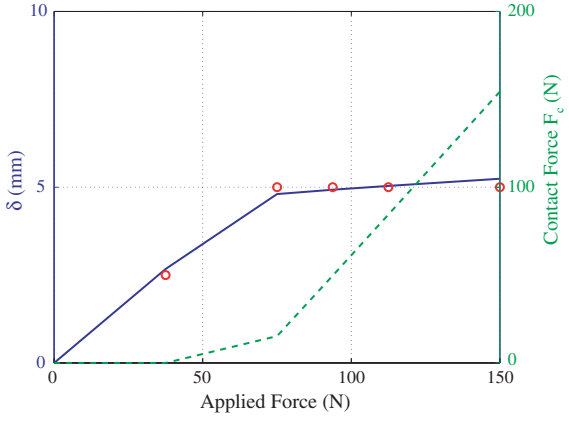

Fig. 22. Performance characteristics of the displacement delimited gripper.

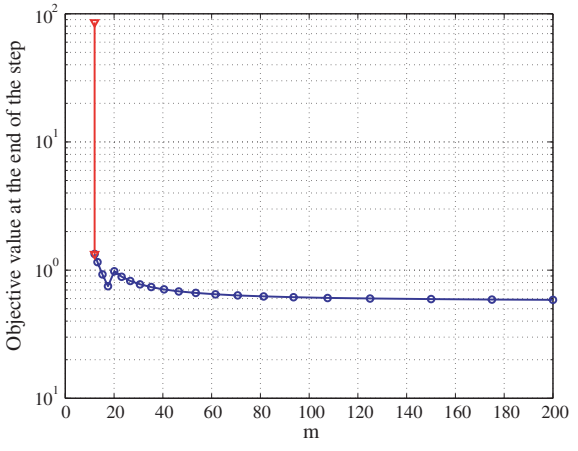

Fig. 23. Convergence history for the displacement delimited gripper.

components of the output path are shown separately in Fig. 25 to emphasize the locking of the output Y displacement.

7.4. Mechanical frequency doubler

Oscillator circuits are used to generate harmonic multiples of a base signal in a variety of electronic applications. A mechanical implementation of a frequency doubler is the objective of this design example. Exploiting the symmetry of the problem, only one-half of the design domain will be shown in the following figures. The schematic for the synthesis problem is shown in Fig. 26. As in example three, an artificial spring is added at the output port and the objective defined by (Eq. (13)) is used in the optimization process.

The result from the synthesis procedure is shown in Fig. 27. The designed value of the gap at the contact node is 18.9 mm.

The convergence history for the optimization is shown in Fig. 28, while the performance of the design is summarized in Fig. 29. The first half of the input cycle in Fig. 29 is the loading half; the input is gradually unloaded over the next half-cycle to return to the original configuration. The response corresponding to only the

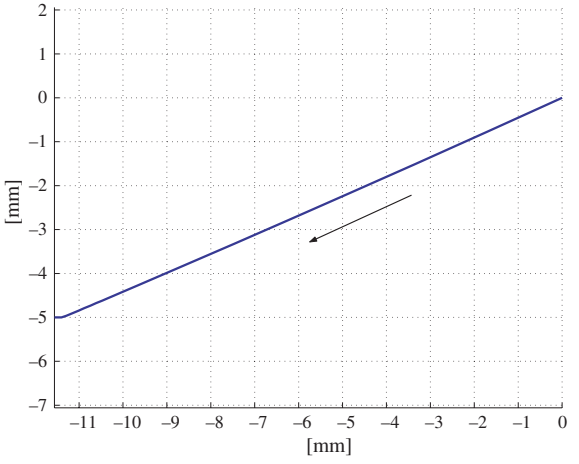

Fig. 24. The path for the output port of the displacement delimited gripper as simulated by nonlinear FEA using ABAQUS.

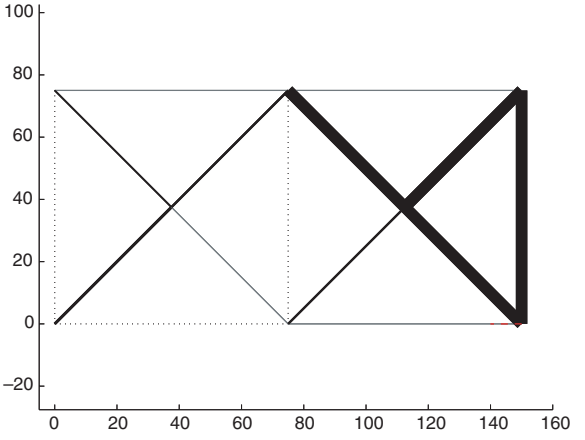

Fig. 27. The design for a mechanical frequency doubler obtained from the synthesis procedure. The axes are marked in mm.

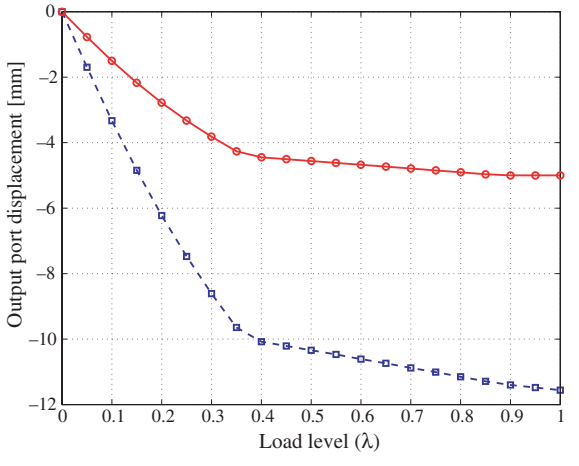

Fig. 25. The X displacement (dashed black curve with squares, blue) and the Y displacement (solid gray red curve with circles, red) of the output port for the final design. (For interpretation of the references in colour in this figure legend, the reader is referred to the web version of this article.)

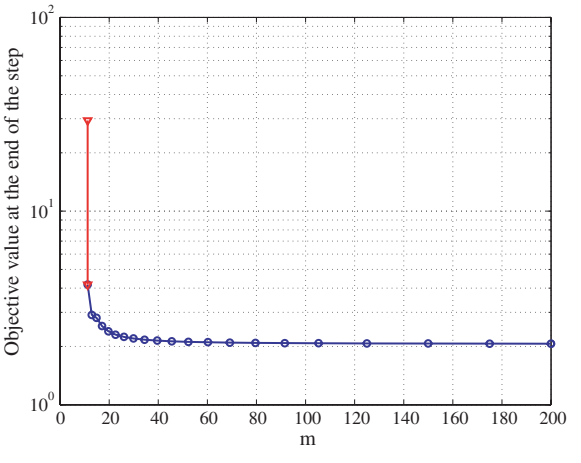

Fig. 28. The convergence history for the mechanical frequency doubler.

loading half of the applied load cycle is shown in Fig. 29 as the response corresponding to unloading part is a

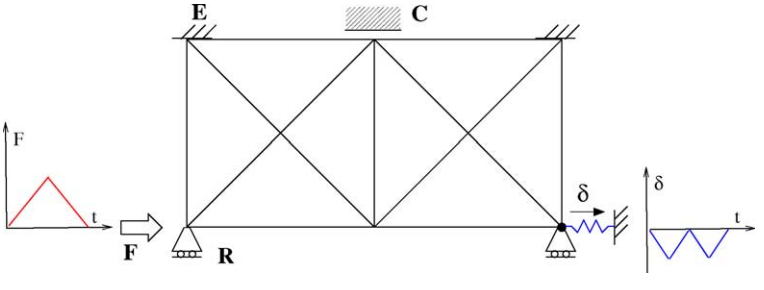

Fig. 26. Schematic of the problem formulation for the mechanical frequency doubler. The output node displacement (δ) is positive in the direction shown by the arrow.

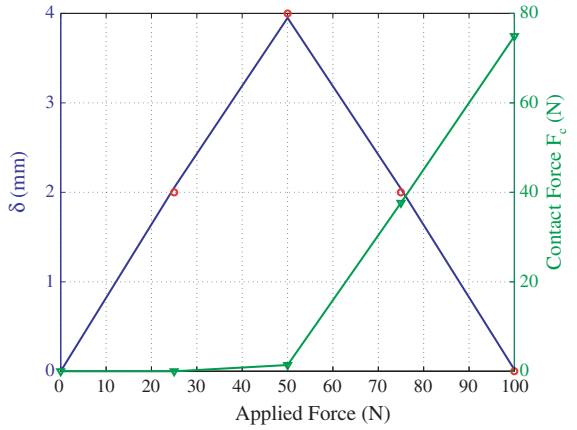

Fig. 29. Performance characteristics of the mechanical frequency doubler (one-half of the input cycle).

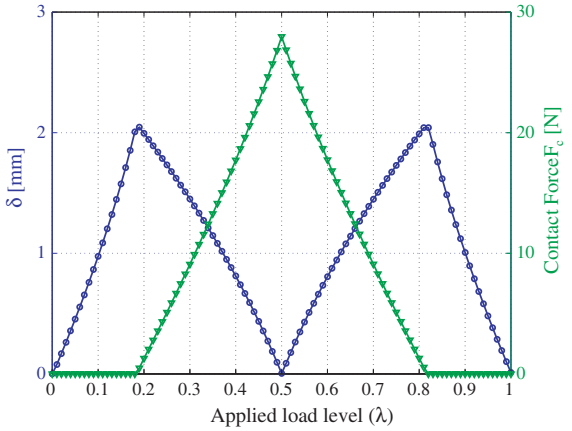

Fig. 30. Performance characteristics of the modified mechanical frequency doubler obtained from geometrically nonlinear FEA in ABAQUS.

mirror image of this about the $Y = 100$ N line. The solid black curve represents the actual force–deflection characteristics of the final design. The specified characteristics are overlaid in hollow gray dots (red). The contact reaction at the only contact node is also plotted in solid gray curve with triangles (green) to the scale shown at the right. Instead of δ, $(-\delta)$ is plotted to the scale on the left for convenience. Note that one full output cycle of amplitude 3.95 mm is obtained for the half-input cycle.

The amplitude of the input port displacement for this design, as predicted by linear FEA is approximately 40 mm, which is approximately 25% of the linear dimension of the design domain. Therefore, the design is more appropriately analyzed by geometrically nonlinear FEA. It is observed that linear FEA overestimates the displacements at the output and contact nodes. Therefore, the behavior of this design for the geometrically nonlinear analysis is very different from that predicted by geometrically linear analysis. However, the topology of the design is consistent with the qualitative behavior indicated by the linear analysis. It is therefore instructive to explore the feasibility of modifying this design to yield the desired behavior for geometrically nonlinear analysis. The gap at the contact node was reduced to 7.0 mm so that the gap is closed during the nonlinear analysis at approximately the same load level at which it is closed in the linear analysis. The amplitude of the output waveform for this modified design is approximately 2.0 mm as plotted in Fig. 30. The solid black curve with hollow dots represents the actual force–deflection characteristics of the modified design. The contact reaction is also plotted in solid gray curve with triangles to the scale shown at the right. The results are plotted for a full applied load cycle. Comparing the performance characteristics in Figs. 29 and 30, it is observed that large displacements and rigid-body rotations mar the symmetric nature of the output waveform but retain the essential features. The path of the contact node is plotted in Fig. 31. The uneven spacing for the markers results from an overlap of the forward and return paths. The left pane of Fig. 32 shows the experimental setup for testing a polypropylene prototype of the modified design. A stepper motor and a Basic Stamp microcontroller are used to actuate the prototype, while a linear Hall-effect sensor is used to measure the displacement of the output port in a noninvasive manner. The white strips corresponding to the contact surface are lined with Teflon to reproduce the frictionless contact assumption underlying the design. The output displacement recorded for a sequence of three input cycles is shown in the right pane of Fig. 32.

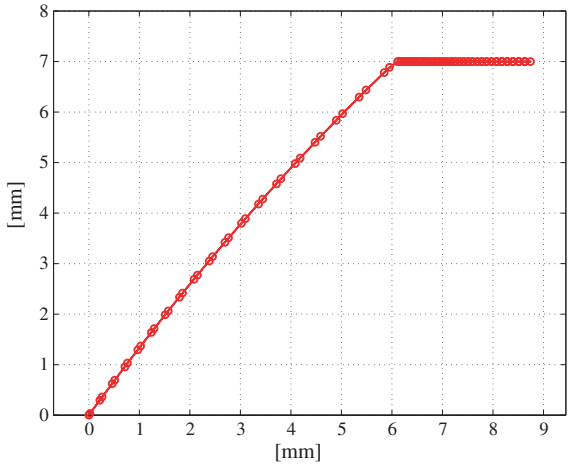

Fig. 31. The path of the contact node for the modified mechanical frequency doubler as predicted by geometrically nonlinear FEA in ABAQUS.

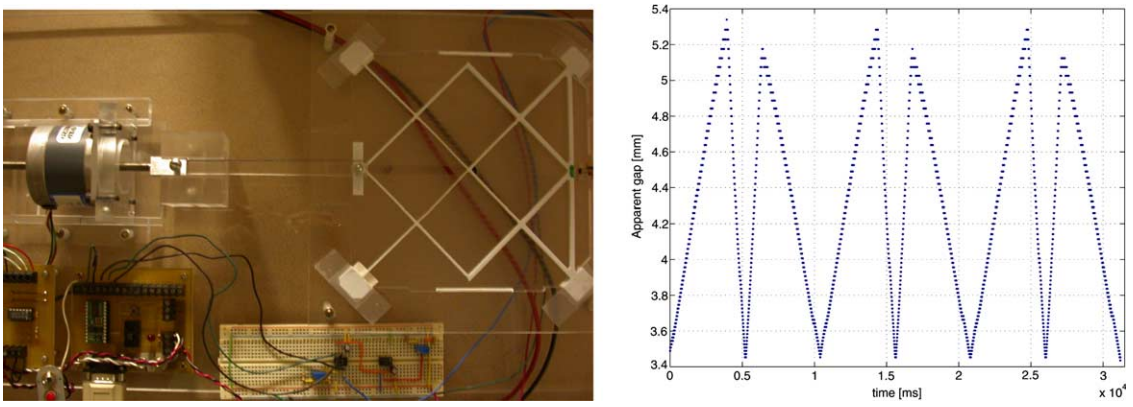

Fig. 32. Experimental setup to test a polypropylene prototype of the mechanical frequency doubler (left) and output displacement corresponding to three input cycles (right).

8. Discussion and future work

As a single problem is decomposed into a series of problems that are solved sequentially, the usefulness of the approach outlined in this paper depends on the computational cost of the procedure. The convergence histories of the design examples show that most of the objective reduction is accomplished during the initial one or two steps, when the sharpness (m) is small. The rest of the steps refine this solution to make it consistent with the actual mechanics of contact. The convergence history from the mechanical OR gate example is shown in Fig. 33 as an example. The steps in the sequential optimization are identified by the value of the sharpness parameter (m) laid off on the x-axis. The y-axis on the left is marked in terms of the number of objective function calls need to solve the optimization sub-problem for a step of the sequential process. The y-axis on the right is marked in terms of number of iterations needed by the optimization algorithm to solve that sub-problem.

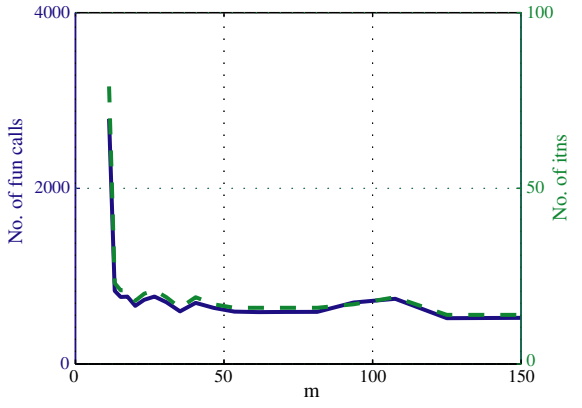

Fig. 33. The number of objective function calls and iterations for each step of the sequential optimization process for the mechanical OR gate example.

The two parameters that control the sequential optimization process are the initial sharpness (m_0) and the rate of increment (Δm). Numerical experiments indicated that the choice of an appropriate m_0 is more important than the choice of Δm. A low level of sharpness (or equivalently, a high level of smoothening) increases the range of validity of the local approximation constructed by the optimization algorithm, especially around the onset of contact (e.g. see Fig. 6b). However, this also implies a higher 'contact reaction' before the physical onset of contact. If the initial (i.e. zero external load) contact reaction is of a magnitude that causes a response, which is comparable to that caused by the applied forces, the corresponding state solution is too removed from the mechanics of contact. Such a choice of m_0 would lead to wasteful computations at best and yield a poor solution in the worst case. As seen from Fig. 6b, for low m, the slope (k_s) of the 'contact reaction' is significant. Therefore even if the magnitude of the 'contact reaction' is small, as controlled by the choice of m_0, the optimization algorithm is able to explore the potential use of contact by varying the gap variable. Sharpness increment rates (Δm) of 10%, 15% and 20% were found to yield almost identical results. A larger rate of increment resulted in fewer steps in the sequential optimization process, but this was offset by increased number of optimization iterations for each step. Hence, Δm of 15% was used for all examples.

The small displacement assumption in conjunction with smoothness of the contact boundary at potential contact nodes has been used to justify the substitution of the contact surface normal by the rigid surface normal ($\hat{\mathbf{n}}$) at the corresponding point in Eq. (4) (see Fig. 4). Though this is an approximation, it is not a concern in practical realizations of CCMs with few nodal or point

contacts. In practical CCM designs, the contact interface geometry can be suitably modified in a post-processing step without altering the topology of the mechanism. For the same reason, the detection of contact can be done at the beam centerline instead of on the actual contact edge in the contact analysis for the small displacements case.

The assumption of small displacements makes it possible to use geometrically linear FEA to simulate the behavior of a candidate design in the optimization procedure. While a number of interesting CCMs with practically useful force–deflection responses can be designed without overstepping the bounds imposed by this assumption, it precludes the design of CCMs for generating prescribed nonsmooth paths. Therefore, a logical extension of this work is to use geometrically nonlinear FEA for the state simulation. This would enable the use of the procedure introduced in this work, for synthesizing nonsmooth path generating CCMs. Unlike the geometrically linear or small displacements case, in the geometrically nonlinear case, the stiffness matrix of the elastic body (i.e. the component $\mathbf{K}$ of the effective stiffness $\mathbf{K}_e$) is also a function of the displacement. Hence, though the solution procedure in Eq. (10) remains unchanged, both $\mathbf{K}$ and $\mathbf{K}_s$ need to re-evaluated for every increment and/or iteration.

It should also be noted that the correspondence between the response value and the input force value for a precision point in the desired response is not always necessary from the viewpoint of mechanism functionality. Ullah and Kota [47] note that, in the context of the synthesis of path and function generating rigid-body mechanisms, this correspondence places an artificial constraint on the optimization procedure and thereby, restricts the feasible domain. They use rigid-body motion and scale invariant shape descriptors along with a corresponding partition of the design variables to separate the shape and size requirements of a specified response, which are then addressed separately. Adaptation of this approach for synthesis of path generating CCMs can also be explored.

9. Conclusions

Contact-aided compliant mechanisms (CCMs) enhance the functional capabilities of CMs by enabling nonsmooth responses. An extension of the technique of topology optimization, which has been used widely for synthesis of compliant mechanisms (CMs), for systematic synthesis of CCMs was introduced in this work. The synthesis procedure used for CMs, cannot be used directly for the synthesis of CCMs due to the nondifferentiability of the response of a CCM at certain irregular points in the design domain.

A smoothened contact model, based on hypothetical nonlinear springs, is introduced to *regularize* the contact analysis under the assumptions of small displacements and frictionless, adhesionless contact. A *generalized step function* is used to model the stiffness of the hypothetical contact spring as a function of the proximity of the contacting body to an external contact surface. Although this function is chosen for mathematical properties that make the numerical solution robust, it can also be interpreted as an analytical constitutive contact relation, which approximates phenomenological contact relations obtained by other researchers. A single scalar parameter (m) in the smoothened contact model is used to characterize the amount of smoothening introduced into the contact analysis. Thus, the smoothened contact model yields a parametric smoothened approximation of the actual contact analysis problem. Variation of the parameter (m) produces a sequence of problems that approach the actual problem as $m \to \infty$. This is exploited to make the optimization-based synthesis procedure more robust by decomposing the problem of CCM synthesis into sequential optimization of a series of approximate sub-problems, which are characterized by increasing m. This *state continuation* approach not only makes the problem amenable to smooth optimization algorithms, but also decreases the likelihood of the algorithm getting trapped in local minima. A number of design examples are solved to illustrate the ability of the procedure to generate CCM designs systematically for prescribed nonsmooth responses using smooth optimization algorithms. Extensions of this work to address nonsmooth path generating CCMs are also discussed briefly.

Acknowledgements

This work was supported by NSF grant DMI0200362. This support and useful discussions with Professors John Bassani and Vijay Kumar (University of Pennsylvania) and Ken Johnson (University of Cambridge) are gratefully acknowledged. We are thankful to Mr. B. Balogh and T. Kientz for their help with fabricating and testing the designs.

References

[1] Midha A. Elastic mechanisms. In: Erdman AG, editor. Modern kinematics—the developments in the last 40 years. John Wiley & Sons; 1993 [chapter 9].
[2] Ananthasuresh GK, Kota S. Designing compliant mechanisms. Mech Eng, ASME 1995;117(11):93–6.
[3] Howell LL. Compliant mechanisms. Wiley Interscience Publications, John Wiley & Sons; 2001.

[4] Moulton T, Ananthasuresh GK. Design and manufacture of electro-thermal-compliant micro devices. Sens Actuators, Phys 2001;90(1–2):38–48.
[5] Erdman AG, Sandor GN, Kota S. Mechanism design: analysis and synthesis. 4th ed. Prentice-Hall; 2001.
[6] Mankame ND, Ananthasuresh GK. Contact aided compliant mechanisms: concept and preliminaries. CD-ROM Proceedings of the ASME DETC2002. Paper # MECH-34211, 2002.
[7] Ananthasuresh GK, Frecker MI. Optimal synthesis with continuum models, in Ref. [3], 2001 [chapter 9].
[8] Hilding D, Klarbring A, Petersson J. Optimization of structures in unilateral contact. Appl Mech Rev 1999; 52(4):139–60.
[9] Mijar AR, Arora JS. Review of formulations for elastostatic frictional contact problems. Struct Multidiscip Optim 2000;20(3):167–89.
[10] Klarbring A, Rönqvist M. Nested approach to structural optimization in non-smooth mechanics. Struct Optim 1995;10:79–86.
[11] Klarbring A, Petersson J, Rönqvist M. Truss topology optimization including unilateral contact. J Optim Theory Appl 1995;87:1–31.
[12] Saxena A, Ananthasuresh GK. Topology synthesis of compliant mechanisms for nonlinear force–deflection and curved path specifications. J Mech Des, Trans ASME 2001;123(1):33–42.
[13] Pedersen CBW, Buhl T, Sigmund O. Topology synthesis of large-displacement compliant mechanisms. Int J Numer Methods Eng 2001;50:2683–705.
[14] Mankame ND, Ananthasuresh GK. A novel compliant mechanism for converting reciprocating translation into enclosing closed paths. ASME J Mech Des, in press.
[15] Kikuchi N, Oden JT. Contact problems in elasticity: a study of variational inequalities and finite element methods. In: SIAM studies in applied mathematics. Philadelphia: SIAM; 1988.
[16] Harker PT, Pang J-S. Finite dimensional variational inequalities and linear complementarity problems. Math Programming 1990;48:161–220.
[17] Chen C, Mangasarian OL. A class of smoothing functions for nonlinear and mixed complementarity problems. Comput Optim Appl 1996;5:97–138.
[18] Oden JT, Pires EB. Nonlocal and nonlinear friction laws and variational principles contact problems in elasticity. J Appl Mech 1983;50:67–76.
[19] Zavarise G, Wriggers P, Schrefler BA. A method for solving contact problems. Int J Numer Methods Eng 1998; 42:473–98.
[20] Wriggers P. Computational contact mechanics. Chichester, UK: John Wiley & Sons; 2002.
[21] Li W, Li Q, Steven GP, Xie YM. An evolutionary shape optimization procedure for contact problems in mechanical design. J Mech Eng Sci, Proc IME, Part C 2003; 217(C4):435–46.
[22] Belegundu AD, Chandrupatla TR. Shape optimization of valve geometry with contact analysis. In: Saigal S, Mukjerjee S, editors. Sensitivity analysis and optimization with numerical methods. New York: ASME; 1990. p. 71–8.
[23] Hilding D, Torstenfelt B, Klarbring A. A computational methodology for shape optimization of structures in frictionless contact. Comput Methods Appl Mech Eng 2001;190:4043–60.
[24] Zabaras N, Bao Y, Srikanth A, Frazier WG. A continuum sensitivity analysis for metal forming processes with application to die design problems. Int J Numer Methods Eng 2000;48:679–720.
[25] Frecker MI, Ananthasuresh GK, Nishiwaki S, Kikuchi N, Kota S. Topological synthesis of compliant mechanisms using multi-criteria optimization. J Mech Des, Trans ASME 1997;119(2):238–45.
[26] Benedict RL, Taylor JE. Optimal design for elastic bodies in contact. In: Haug EJ, Cea J, editors. Optimization of distributed parameter structures, 2. Holland: Sijthoff and Noordhoff Publishers; 1981. p. 1553–99.
[27] Klarbring A. On the problem of optimizing contact force distributions. J Optim Theory Appl 1992;74:131–50.
[28] Hilding D. A heuristic smoothing procedure for avoiding local optima in optimization of structures subject to unilateral constraints. Struct Multidiscip Optim 2000;20:29–36.
[29] Park J, Anderson WJ. Geometric optimization in the presence of contact singularities. AIAA J 1995;33:1503–9.
[30] Petersson J, Patriksson M. Topology optimization of sheets in contact by a subgradient method. Int J Numer Methods Eng 1997;40:1295–321.
[31] Stavroulakis GE. Optical prestress of cracked unilateral structures: finite element analysis of an optimal control problem for variational inequalities. Comput Methods Appl Mech Eng 1995;123:231–46.
[32] Outrata J, Zowe J. Numerical approach to optimization problems with variational inequality constraints. Math Programming 1995;68:105–30.
[33] Tin-Loi F. On the numerical solution of a class of unilateral contact structural optimization problems. Struct Multidiscip Optim 1999;17:155–61.
[34] Facchinei F, Jiang H, Qi L. A smoothing method for mathematical programs with equilibrium constraints. Math Programming 1999;85:107–34.
[35] Kim NH, Park YH, Choi KK. Optimization of a hyperelastic structure with optimization multibody contact using continuum-based shape design sensitivity analysis. Struct Multidiscip Optim 2001;21:196–208.
[36] Saxena A, Ananthasuresh GK. On an optimal property of compliant topologies. Struct Multidiscip Optim 2000;19: 36–49.
[37] Bendsøe MP, Sigmund O. Topology optimization: theory, methods and applications. New York: Springer; 2003.
[38] Belegundu AD, Chandrupatla TR. Introduction to finite elements in engineering. 2nd ed. Upper Saddle River, NJ, USA: Prentice-Hall; 1997.
[39] Ortega JM, Rheinboldt WC. Iterative solution of nonlinear equations in several variables. New York: Academic Press; 1970.
[40] Bendsøe MP, Olhoff N, Sokolowski J. Sensitivity analysis of problems of elasticity with unilateral constraints. J Struct Mech 1985;13(2):201–22.
[41] Crisfield MA. In: Nonlinear finite element analysis of solids and structures, vol. 1. John Wiley & Sons; 1991.
[42] Bergstrom PL, Tamagawa T, Polla DL. Design and fabrication of micromechanical logic elements. In: Proceedings of the 1990 IEEE Micro Electro Mechanical Systems conference, Napa Valley, CA, 1990. p. 15–20.

[43] Sigmund O. On the design of compliant mechanisms using topology optimization. Mech Struct Mach 1997;25(4):493–524.

[44] Mankame ND, Ananthasuresh GK. Topology synthesis of electrothermal compliant (ETC) mechanisms using line elements. In: Proceedings of the 2001 ASME Design Engineering Technical Conferences, Pittsburgh, 2001, Paper no. DETC2001/DAC-21019.

[45] Bruns TE, Tortorelli DA. Topology optimization for nonlinear elastic structures and compliant mechanisms. Comput Methods Appl Mech Eng 2001;190(26–27):3443–59.

[46] Dzeidzic R, Frecker MI. Design of multifunctional compliant mechanisms for minimally invasive surgery—preliminary results. In: Proceedings of the 2001 ASME Design Engineering Technical Conferences, Symposium on Mechanisms and Devices for Medical Applications, Pittsburgh, 2001, Paper no. DETC2001/DAC-21055.

[47] Ullah I, Kota S. Optimal synthesis of mechanisms for path generation using fourier descriptors and global search methods. ASME J Mech Des 1997;119:504–10.